Geoderma 402 (2021) 115355

Contents lists available at ScienceDirect

Geoderma

journal homepage: www.elsevier.com/locate/geoderma

Pedogenesis and carbon sequestration in transformed agricultural soils of Sicily

Markus Egli [a,*,1], Michèle Bösiger [a,1], Krzysztof Lamorski [c], Cezary Sławiński [c], Michael Plötze [d], Guido L.B. Wiesenberg [a], Dmitry Tikhomirov [a], Alessandra Musso [a], Shao-Yiu Hsu [e], Salvatore Raimondi [b]

[a] Department of Geography, University of Zürich, CH-8057 Zürich, Switzerland
[b] Department of Agricultural, Food and Forest Sciences, University of Palermo, 90128 Palermo, Italy
[c] Institute of Agrophysics, Polish Academy of Sciences, Doświadczalna 4, 20-290 Lublin, Poland
[d] Institute for Geotechnical Engineering, ETH Zurich, Stefano-Franscini-Platz 5, 8093 Zurich, Switzerland
[e] Department of Bioenvironmental Systems Engineering, National Taiwan University, Taipei 10617, Taiwan

ARTICLE INFO

Handling Editor: Ingrid Kögel-Knabner

Keywords:
Soil formation
Weathering
Carbon sequestration
Soil transformation
Mediterranean
CO_2

ABSTRACT

The increasing atmospheric CO_2 concentration is a consequence of human activities leading to severe environmental deteriorations. Techniques are thus needed to sequester and reduce atmospheric carbon. One of the proposed techniques is the transformation or construction of new soils into which more organic carbon can be sequestered and CO_2 be consumed by increased weathering. By using a chronosequence of new and transformed soils on crushed limestone (0–48 years) in a Mediterranean area (Sicily), we tried to quantify the amount of organic carbon that could be additionally sequestered and to derive the corresponding rates. A further aim was to trace chemical weathering and related CO_2 consumption and the evolution of macropores that are relevant for water infiltration and plant nutrition. Owing to the irrigation of the table grape cultivation, the transformed soils developed fast. After about 48 years, the organic C stocks were near 12 kg m^{-2}. The average org. C sequestration rates varied between 68 and 288 g m^{-2} yr^{-1}. The C accumulation rates in the transformed soils are very high at the beginning and tend to decrease over (modelled) longer time scales. Over these 48 years, a substantial amount of carbonate was leached and reprecipitated as secondary carbonates. The proportion of secondary carbonates on the total inorganic carbon was up to 50%. Main mineralogical changes included the formation of interstratified clay minerals, the decrease of mica and increase of chloritic components as well as goethite. The atmospheric CO_2 consumption due to silicate weathering was in the range of about 44–72 g C m^{-2} yr^{-1}. Due to the high variability, the contribution of chemical weathering to CO_2 consumption represents only an estimate. When summing up organic C sequestration and CO_2 consumption by silicate weathering, rates in the order of 110–360 g C m^{-2} yr^{-1} are obtained. These are very high values. We estimated that high sequestration and CO_2 consumption rates are maintained for about 50–100 years after soil transformation. The macropore volume decreased over the observed time span to half (from roughly 10 to 5 %). The transformation of soils may even amend their characteristics and increase agricultural production. Due to the relatively sandy character, enough macropores were present and no substantial compaction of the soils occurred. However, great caution has to be taken as such measures can trigger deterioration of both soil ecosystem services and soil quality.

1. Introduction

The increasing atmospheric content of CO_2 is a consequence of human activities and is associated with severe and threatening climate change. It is more than evident that climate change creates additional stress on land, exacerbating existing risks to livelihoods, biodiversity, human and ecosystem health, infrastructure, and food systems (IPCC, 2020). Many strategies for combatting soil overuse or desertification can contribute to climate change adaptation. Avoiding, reducing and reversing soil overuse and promoting sustainable land use would

* Corresponding author.
E-mail address: markus.egli@geo.uzh.ch (M. Egli).
[1] Contributed equally to the paper and share first authorship.

https://doi.org/10.1016/j.geoderma.2021.115355
Received 8 April 2021; Received in revised form 19 June 2021; Accepted 16 July 2021

Table 1
Description of the investigated sites.

Profile	Coordinates	Altitude (m a.s.l.)	MAAT (°C)	MAP (mm)	Slope (%)	Exposure	Parent material	WRB Soil taxonomy	Land use	Year of transformation
1) Canicattì area										
Grotta	37° 24′30.2″N/	519	16	600	1	150°	Limestone	Luvisol	Orchard:	–
Rossa 4a1	13° 53′27.0″E						(Calcare di base)		Table grapes (Uva da tavola)	
Grotta	37° 24′29.6″N/	515	16	600	10	150°	Limestone	Anthrosol	Orchard:	1975
Rossa 2a1	13° 53′28.8″E						(Calcare di base)		Table grapes (Uva da tavola)	
Grotta	37° 24′27.0″N/	511	16	600	16	150°	Limestone	Anthrosol	Orchard:	1975
Rossa 2a2	13° 53′27.0″E						(Calcare di base)		Table grapes (Uva da tavola)	
Cazzola 4	37° 21′57.7″N/	459	16	600	3	150°	Limestone	Anthrosol	Orchard:	1985
	13° 48′04.7″E						(Calcare di base)		Table grapes (Uva da tavola)	
C.Fazio	37° 24′07.5″N/	514	16	600	5	75°	Limestone	Anthrosol	Orchard: Table	1993
	13° 52′14.0″E						(Calcare di base)		grapes (Uva da tavola) and peach	
C.Fazio 2	37° 24′04.4″N/	524	16	600	8	335°	Limestone	Anthrosol	Orchard:	1993
	13° 52′15.7″E						(Calcare di base)		Table grapes (Uva da tavola)	
Lauria P1a	37° 19′05.0″N/	387	16	600	10	10°	Limestone	Anthrosol	Orchard:	2003
	13° 54′43.0″E						(Calcare di base)		Table grapes (Uva da tavola)	
Lauria P1	37° 19′15.0″N/	375	16	600	12	10°	Limestone	Anthrosol	–	2020
	13° 54′43.0″E						(Calcare di base)			
2) Mazara del Vallo area										
Mazara del	37° 43′06.3″ N/	63	18	500	–	–	Limestone	Regosol	pasture	–
Vallo Ferla	12° 35′ 13.1″ E						(Calcarenite)			
Mazara del	37° 43′20.7″ N/	63	18	500	–	–	Limestone	Anthrosol	Orchard:	1972
Vallo P7	12° 35′ 04.3″ E						(Calcarenite)		Table grapes(Uva da tavola)	
Mazara del	37° 43′10.5″ N/	63	18	500	–	–	Limestone	Anthrosol	Orchard:	1975
Vallo P4	12° 35′ 19.4″ E						(Calcarenite)		Table grapes (Uva da tavola)	

enhance soil fertility, increase carbon storage in soils and biomass, while agricultural productivity and food security may also benefit. Many sustainable land management practices are not widely adopted due to insecure land tenure, lack of access to resources and agricultural advisory services, insufficient and unequal private and public incentives, and lack of knowledge and practical experience (IPCC, 2020). Soil management is only then sustainable when a green area whose natural or artificial development (as a consequence of green operations) produces wealth and/or does not cause any damage to people, animals, plants, soil and movable and immovable objects (Raimondi et al., 2020).

In this context, the international 4 per 1000 initiative steps in by supporting states and non-governmental stakeholders in their efforts towards a better management of soil carbon stocks (Dignac et al., 2017). The soil organic carbon abundance depends on soil C inputs and outputs. Input, output, storing mechanisms and C-budget are a result of spatially interconnected processes that are strongly influenced by human activities. To increase carbon sequestration and follow the main goal of this initiative, changes in land use would be needed in many places. Such changes are not only related to soil management but may also include the restoration of soils to stabilise and even increase carbon sequestration. An increased and steady soil carbon/soil organic matter storage would help to improve soil fertility and agricultural productivity (see also the 4 per 1000 initiative; http://4p1000.org/).

Young natural or artificial soils accumulate organic carbon at high rates (Egli et al., 2001; Egli et al., 2012; Gerwin et al., 2011; Elmer et al., 2013; Vilmundardóttir et al., 2015). Depending on climate, carbon and nitrogen stocks in natural soils tend to reach a quasi-steady state after about 4 to 10 kyr (Egli et al., 2012). In very young soils (age < 100 years), carbon sequestration rates vary between about 3 to 100 g m^{-2} yr^{-1}. In young soils having primary silicate minerals, chemical weathering reactions consume a high amount of CO_2 (Urey reaction; Blättler and Higgins, 2017). Furthermore, the absorption capacity of organic C is in young soils not reached enabling them to bind organic matter at high rates. Therefore, if weathering in agricultural soil is promoted, more atmospheric CO_2 can be consumed or absorbed as organic matter in soils. By adding rock material (or powder) to soils, weathering will be enhanced. Untreated surfaces have weathered over many millennia and available reaction partners are already consumed or relocated to deeper soil horizons, where a direct exchange with the atmosphere is no longer possible (Porder, 2019). Andrews and Taylor (2019) stated that enhanced weathering of silicate rocks is a carbon dioxide removal technology that may be capable of removing sizeable quantities of CO_2 from the atmosphere relatively rapidly and, therefore, help mitigate anthropogenic climate change. According to Köhler et al. (2010), Taylor et al. (2017) or Andrews and Taylor (2019) enhanced weathering of silicate and calcareous rock potentially could remove up to 30 Pg C $year^{-1}$ from the atmosphere (which would be equal to a global temperature decrease of 0.2 °C–1.6 °C by the year 2100). However, the current understanding of enhanced weathering is largely based on previous studies of long-timescale natural chemical weathering. The true ability of enhanced weathering to sequester atmospheric CO_2 still has to be explored and depends on a multitude of weathering pathways and biogeochemical interactions.

In several countries, soil amendment techniques are increasingly being used owing to economic competition, degraded soils and to cope with the higher demand on food. In several countries strict regulations exist as to how soil amendments have to be done. The use of unweathered material on top of an existing soil without the addition of a B- and A-horizon and a clear soil stratigraphy is in some countries even not allowed or difficult to be achieved (FSKB, 2021), because the focus is on soil protection and prevention of compaction: – something that probably should be reconsidered under a broader aspect in future. In the Mediterranean and particularly in Sicily and Puglia, soil transformations are widely applied. Pedotechniques are currently used to generate soils suitable for table grape cultivation in order to increase productivity and grape quality, and, thus, to get substantial financial returns (Dazzi et al.,

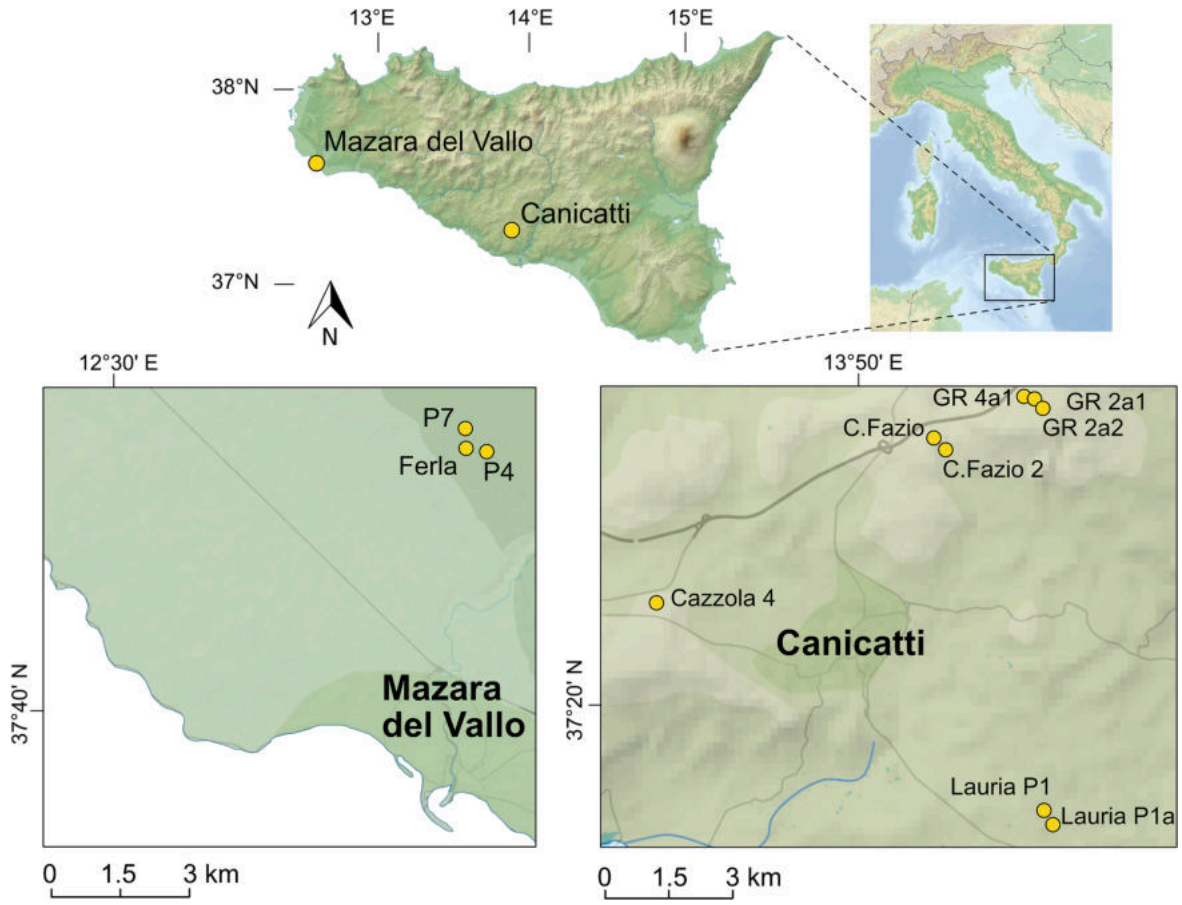

Fig. 1. Overview of the investigation areas and plots (GR = Grotta Rossa). Source: Wikimedia, Tschubby.

2019). Soil transformations are relatively costly. The higher productivity and the subsequently higher profitability of the cultivation often amortise the start-up costs (Dazzi et al., 2019).

The main focus of this investigation lies on the estimation/quantification of atmospheric carbon that can be additionally sequestered with transformed soils in a Mediterranean area (Sicily). Consequently, we have the following research questions: i) How much organic carbon has been stored after soil transformation?, ii) Which are the sequestration rates and is a saturation reached after a certain time?, iii) How does the soil structure (pores), relevant for water percolation and plant nutrition, develop over time?, iv) Is silicate weathering detectable and was carbonate leached or secondary carbonates formed?

2. Sampling strategy and study sites

2.1. Sampling strategy

The time over which natural weathering and accumulation of soil organic carbon occurs usually cannot be observed and reproduced by experimental or laboratory studies (see White and Brantley, 2003). To overcome this fundamental restriction the comparative space-for-time-approach has been developed (see e.g. 'soil-landscape chronograms' in Birkeland and Burke, 1988). Chronosequences are, thus, useful for estimating field weathering rates with respect to elemental leaching, mineral transformation or soil organic C accretion (e.g., Álvaro-Fuentes et al., 2014). Consequently, we selected sites where soil transformation having the same material was performed but at a different time. We were able to find 10 sites covering a time span of about 5 decades (from the most recent to the oldest soil transformation; Table 1). We tried to keep the other soil-forming factors, except time, as similar as possible: all sites had a comparable 'parent' material (crushed rocks; arenitic limestone), land use (mostly table grapes) and climate. The topography (slope) showed some minor differences between the sites with some being rather at a flat position and others at the upper part of a uniform slope.

2.2. Study site

The investigated sites are located in central and western Sicily (Canicatti and Mazara del Vallo; Fig. 1). Near the city of Canicatti (province of Agrigento), eight sites with transformed soils were studied and near Mazara del Vallo two transformed sites and one unaffected site. Canicatti has a mean annual precipitation of 600 mm (Arnone et al., 2013) and a mean annual temperature of 16 °C (Viola et al., 2014). The Mazara del Vallo region has an annual precipitation of about 500 mm (Arnone et al., 2013) and an 18 °C mean annual temperature (Viola et al., 2014). The whole region has a Mediterranean climate type.

In Sicily, agricultural production started in the 1990′s to shift in part from vineyards to olive and almond plantations (Raimondi et al., 2020) or legumes such as chickpeas, faba beans and cereal (wheat, barley). Especially in the study regions, however, vineyards and table grapes are cultivated (Table 1). In Sicily, an all-year cultivation is possible in areas having greenhouses and irrigation.

In the area of Canicatti, the farmers normally start to irrigate the area in April with a cycle of 5–9 days. Up to approximately 800–1000 m^3 water m^{-2} yr^{-1} is used until the harvest. With this, the total water input (considering also precipitation) amounts up to about 1300–1600 mm yr^{-1}. Today, irrigation is done via pumps or waterlines which are placed within the grapevine and release water through small openings as drips (Clemente, 1990). Table grapes are annually harvested. The soil is harrowed once a year in March by using a motor hoe for smaller parcels of land, while larger areas are being harrowed by using a tractor

Table 2
Chemical and physical characteristics of the investigated soil profiles.

Site	Horizon	Depth	Munsell colour moist	Skeleton	Bulk density	Sand	Silt	Clay	pH	LOI	Corg	$CaCO_3$	$CaCO_3$(s) [1)]	N	$\delta^{13}C$ (bulk soil)	$\delta^{13}C$ ($CaCO_3$)	C/N ratio	$\delta^{18}O$ ($CaCO_3$)
		cm		wt-%	g cm^{-3}	%	%	%	$CaCl_2$	%	%	%	%	%	‰	‰		‰
1) Canicattì area																		
Grotta Rossa 4a1	Ap	0–40	7.5YR2/3	7.2	1.13	17.0	53.5	29.5	7.50	10.27	2.03	12.6	25.3	0.17	−19.19	−7.01	12	−4.25
(undist.)	Bt	40–80	7.5YR2/3	0.2	1.03	26.3	41.0	32.7	7.42	9.76	1.60	4.9	50.4	0.11	–23.11	−13.00	15	−5.69
Grotta Rossa 2a1	Ap	0–50	7.5YR3/4	49.3	1.41	28.1	48.7	23.1	7.50	6.26	0.83	63.1	12.3	0.08	−7.18	−3.92	10	−3.54
	AC	50–65	10YR4/4	72.3	1.52	38.7	42.6	18.8	7.50	4.48	0.34	72.6	10.2	0.04	−5.27	−3.44	8	−3.54
	C	65–75	2.5Y8/2	25.5	1.15	29.1	58.3	12.7	7.51	2.41	0.21	82.7	16.6	0	−5.12	−4.94		−4.04
Grotta Rossa 2a2	Ap	0–30	10YR4/4	35.5	1.39	23.4	50.0	26.5	7.50	7.18	0.97	60.5	13.5	0.13	−7.01	−4.20	8	−3.29
	Bw	30–85	10YR4/4	32.7	1.31	25.9	49.3	24.8	7.51	7.31	1.14	57.2	15.4	0.07	−7.55	−4.67	18	−3.39
	Ab	85–95	10YR4/4	19.2	1.28	22.5	50.8	26.7	7.50	6.67	1.15	47.3	19.3	0.09	−8.98	−5.59	13	−3.61
Cazzola 4	Ap1	0–40	7.5YR4/4	11.9	1.13	16.8	48.1	35.0	7.5	8.10	0.48	35.1	35.9	0.05	−12.75	−9.54	10	−4.24
	Ap2	40–80	7.5YR4/4	11.2	1.26	16.1	48.9	35.0	7.4	7.46	0.64	33.8	37.3	0.09	−12.38	−9.87	7	−4.35
	Ap3	80–100	7.5YR5/6	25	1.21	23.3	41.0	35.8	7.5	7.22	0.00	34.5	36.7	0.02	−12.29	−9.72		−4.22
C.Fazio	Ap1	0–50	10YR6/3	5.4	1.32	11.0	43.7	45.4	7.48	5.92	0.89	57.4	0.8	0.06	−4.81	−1.18	14	−0.79
	Ap2	50–75	2.5Y5/3	14.9	1.38	10.4	37.9	51.7	7.39	7.97	0.76	25.0	7.5	0.06	−7.66	−2.80	12	−1.83
	Ab	75–85	2.5Y5/4	0.0	1.46	17.2	31.3	51.5	7.37	8.50	0.68	11.9	21.5	0.07	−15.79	−6.11	9	−3.45
C.Fazio 2	Ap1	0–40	2.5Y5/4	4.8	1.4	77.3	8.8	13.9	7.44	7.73	0.63	52.0	0.0	0.15	−5.64	−0.62	4	−0.16
	Ap2	40–70	2.5Y7/3	2.8	1.41	11.7	44.9	43.4	7.51	4.58	0.02	71.5	0.0	0.04	−0.93	−0.20		0.15
	Ap3/Ab	70–80	2.5Y7/4	28.8	1.34	7.7	42.3	50.0	7.57	6.67	0.02	42.1	0.0	0.04	−2.80	−0.77		−0.43
Lauria P1a	AC	0–30	2.5Y5/3	19.6	1.42	47.6	37.7	14.7	7.71	3.31	0.34	82.4	8.8	0.02	−4.32	−3.10	18	−3.35
	C	30–40	2.5Y8/3	14.9	1.72	54.9	38.2	6.9	7.71	1.24	0.00	92.2	2.2	0	−1.99	−1.51		−3.45
Lauria P1	C	0–10	2.5Y8/2	36.8	1.46	62.2	35.1	2.7	7.80	0.74	0.00	96.6	8.1	0.01	−3.16	−2.92		−1.74
2) Mazara del Vallo area																		
Mazara del Vallo	A	0–20	5YR2/4	3.9	1.30	37.5	49.0	13.5	7.35	9.88	2.80	22.6	5.6	0.2	−13.92	−2.33	14	−3.35
Ferla (undist.)	C	20–40	7.5YR5/8	0.0	1.70	63.5	26.1	10.4	7.37	3.08	0.46	83.1	15.0	0.01	−5.40	−4.57		−2.43
Mazara del Vallo	Ap1	0–20	5YR2/4	10.3	1.26	28.4	41.8	29.7	7.32	7.78	1.59	22.5	13.1	0.09	−11.71	−4.10	17	−2.69
P7	Ap2	20–75	5YR2/4	3.0	1.27	30.8	43.9	25.3	7.23	7.08	0.79	24.2	13.0	0.07	−11.08	−4.08	12	−2.56
	C	75–110	5YR3/4	14.4	1.00	34.3	36.1	29.6	7.50	6.19	0.81	34.6	13.4	0.03	−8.19	−4.19	26	−2.45
Mazara del Vallo	Ap	0–50	5YR3/6	20.5	1.26	44.6	35.6	19.9	7.20	5.73	1.74	69.1	13.2	0.11	−7.97	−4.15	16	−3.03
P4	C	50–90	10YR8/6	8.1	1.27	81.3	14.2	4.4	7.57	1.32	0.00	91.2	12.1	0	−4.10	−3.88		−2.83

[1)] proportion of secondary carbonates on total carbonate content.

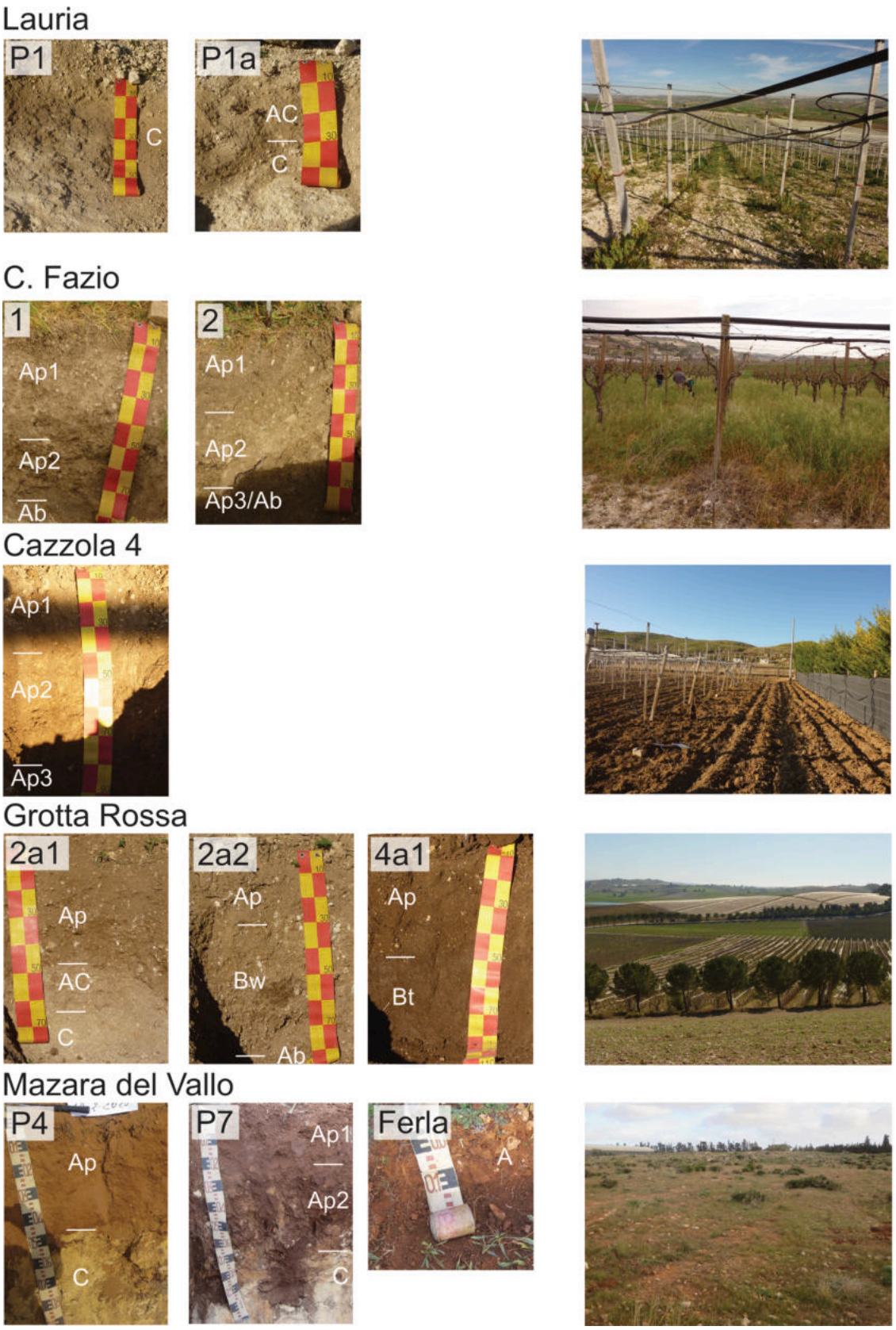

Fig. 2. Photos of the investigated profiles with horizon designations and land use of the area. At all sites, table grapes have been cultivated (since soil transformation). At the undisturbed site Mazara dello Vallo Ferla, pasture is the dominant land use.

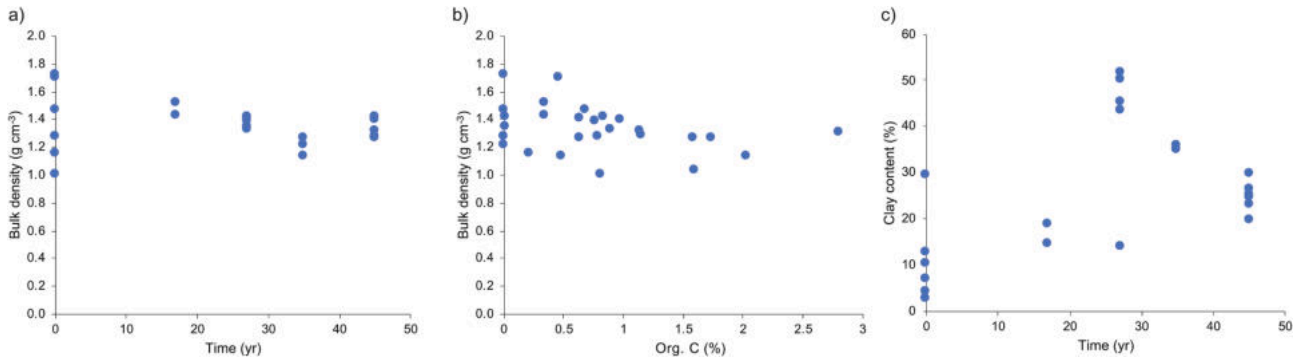

Fig. 3. a) Temporal evolution of bulk density, b) relation between org. C and bulk density and c) increase in the clay content with time.

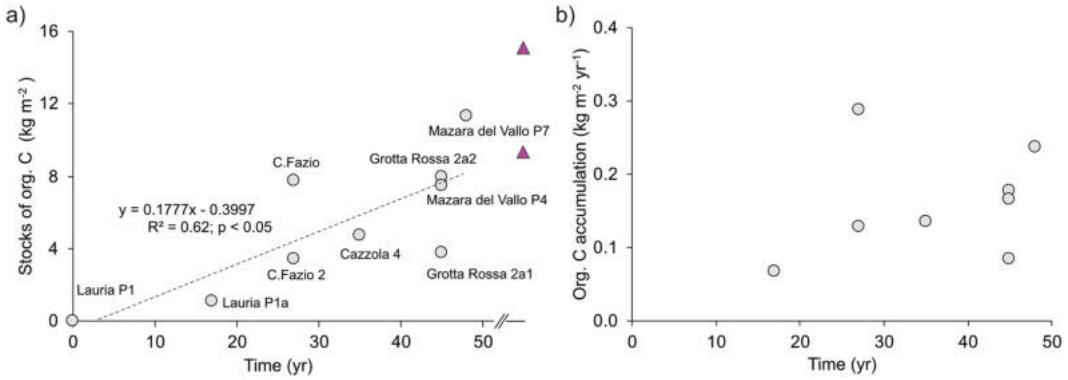

Fig. 4. a) Stocks of organic carbon as a function of time after soil transformation. The triangle represents the unaffected soils at the site Mazara del Vallo Ferla and Grotta Rossa 4a1. The stocks significantly increase (when using a linear regression), b) derived org. C accumulation rates (=stocks/soil age). These rates remain at a high level within the observed time span.

(Lombardo and Raimondi, 1991).

The research area in Canicatti is characterised by an Oligocene to Pliocene geology (Trumpy et al., 2015), with the frequent occurrence of "calcare di base" (limestone). At undisturbed sites Mollisols, Vertisols, Entisols or Aridisols prevail. The soils evolved on typical sediments that were deposited before and during the Messinian Crisis: clayey marine sediments, diatom sediments, limestone (Calcare di Base), detritic deposits and gypsiferous sediments. The Messinian Crisis was responsible for a huge accumulation of evaporites throughout the whole Mediterranean domain (Caruso et al., 2015). Due to soil amendment, frequently Anthrosols on top of former Vertisols can be found.

2.3. Soil sampling

In the Canicatti region, 7 profiles were investigated at sites where new soils were constructed at different times on top of former soils by using crushed rock material (Table 1). The soil constructions and transformations took place between 1975 and 2020. Furthermore, an unaffected soil profile (Grotta Rossa 4a1) was also included. In addition, two sites near Mazara de Vallo were sampled where a soil transformation was performed in 1972. An unaffected profile in Mazara del Vallo was also investigated. We therefore have the possibility to trace how these soils developed over time (over almost 5 decades) and how much carbon has been sequestered. As a further comparison, data of previously in-detail investigated agricultural soils was available (Egli et al., 2020).

At each site, soil pits were dug as deeply as possible either by hand or by using an excavator and were described according to the WRB (IUSS Working Group, 2015). Sampling was done following the horizon sequence along the entire profile down to the underlying former soil (in sites where it was possible). In order to cover soil variability, a large amount (up to 5 kg per sample) of soil material was taken (cf. Hitz et al., 2002).

To determine soil bulk density of each horizon, two – three replicates of 100 cm^3 were taken by using a soil corer to take undisturbed samples. Additional Al-tubes (100 cm^3) were used for the determination of the macropores using X-ray computed tomography (CT).

3. Material and methods

3.1. Chemical analyses of soils

The sampled material was dried for 48 h at 70 °C. It was thereafter gently crushed using a pestle and mortar and sieved to separate the skeleton (>2 mm) from fine earth (<2 mm) fraction. To determine the amount of coarse material, the skeleton was weighed.

Soil pH was determined using a soil-solution (0.01 M $CaCl_2$) ratio of 1:2.5. The oxalate-extractable Al, Fe and Mn content – that usually extracts weakly- and poorly-crystalline phases and some of the organic phases (Mizota and van Reeuwijk, 1989) – was determined following the standard method of McKeague et al. (1971). Element concentrations in the extract were analysed using atomic absorption spectroscopy (AAnalyst 700, Perkin Elmer). The total carbon (C) and nitrogen (N) contents of the bulk soil and $\delta^{13}C$ and $\delta^{18}O$ of bulk soil and carbonates were determined using elemental analysis isotope ratio mass spectrometry (EA-IRMS; Thermo Fisher Scientific Flash HT Plus elemental analyser equipped with a thermal conductivity detector and coupled to a ConFlo lV to Delta V Plus isotope ratio mass spectrometer). The isotopic values were calculated against working in-house standards (Caffeine (Sigma), Chernozem (Black Carbon Reference Materials)), which were themselves calibrated against international reference materials (Caffeine (IAEA 600), Benzoic acid (IAEA 601), Cellulose (IAEA CH3),

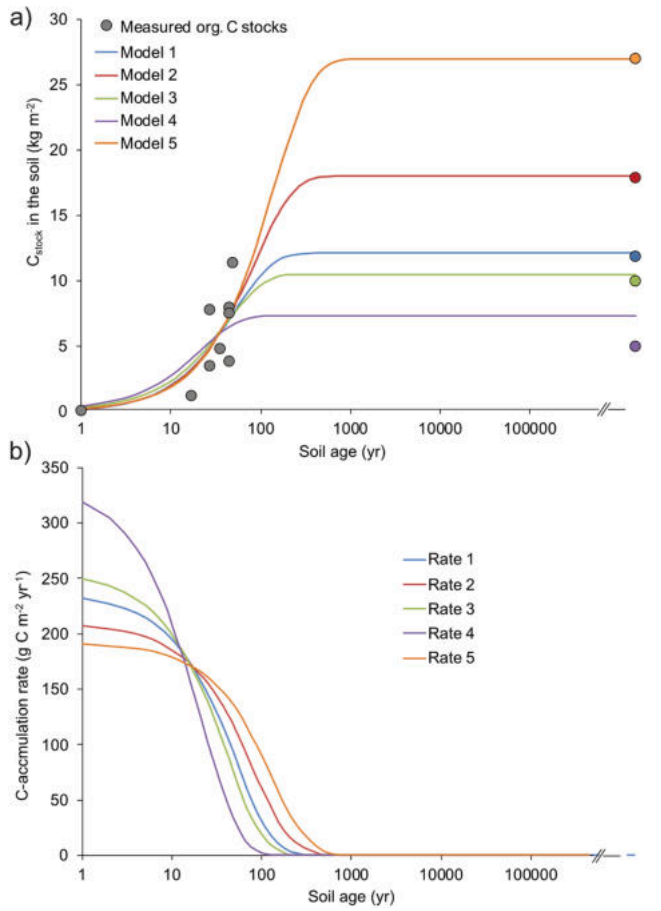

Fig. 5. a) Modelling of org. C stock trends over time using an exponential decay model with $f(t) = a + (b - a)e^{-kt}$ (Lichter, 1998) where a represents an asymptote, b the initial quantity, and k the decay constant. Steady state conditions seem to be reached after about 100–200 years. The model was fitted to typical org. C stocks in agriculture soils in Sicily: Model 1 uses 12 kg C m^{-2} as asymptote (average Mazara del Vallo Ferla, Grotta Rossa 4a1), Model 2 uses 18 kg C m^{-2} as asymptote (average C-stocks on limestone in the area of Canicatti, see Table 7; Egli et al, 2020), Model 3 uses 10 kg C m^{-2} as asymptote (see also Scalenghe et al., 2015; Novara et al., 2017), Model 4 uses 5 kg C m^{-2} as asymptote (see also Scalenghe et al., 2015; Novara et al., 2017) and Model 5 uses 27 kg C m^{-2} as asymptote (typically high stocks near Canicatti, see Table 7; Egli et al, 2020); b) Accumulation rates of org. C obtained from the derivation of the exponential decay functions.

ammonium sulphate (IAEA N1), Urea (IVA)). The carbonate content was determined as described (slightly modified method) in Breitenbach and Bernasconi (2011) using a GasBench-IRMS (Thermo Fisher Scientific GasBench II coupled to Delta V Plus IRMS). Aliquots of samples and standards containing 20–100 μg carbonate C were weighed into exetainer vials, closed and automatically flushed with He for 10 min. 25–50 μl phosphoric acid was added. Samples were measured at least 60 min after acid addition, which was sufficient to release all carbonate C from calcium carbonate, aragonite and dolomite (Breitenbach and Bernasconi, 2011). The carbonate C content and $\delta^{13}C$ and $\delta^{18}O$ values were calibrated against a secondary standard (Merck $CaCO_3$) and international reference material (IAEA NBS18 Calcite). Organic carbon was obtained by the difference between the total and inorganic carbon. To check the reliability of this procedure, the org. C content determined by EA-IRMS was compared to the Walkley-Black method which is thought to give similar results (Gessesse and Khamzina, 2018). Pedogenic carbonate was determined with a rule of three of the $\delta^{13}C$ carb measurements and a corresponding typical $\delta^{13}C$ value of the region for the biogenic material (−24.8 ‰; Egli et al., 2020) and −1 ‰ for 100 % marine carbonate.

The determination of the loss on ignition (LOI; organic matter and adsorbed water) was performed by igniting 2 g of oven-dried fine earth at 550 °C for 6 hr.

The stocks of organic C were calculated using:

$$S_{stock} = \sum_{i=1}^{n} C_i d_i \rho_i (1 - RM) \quad (1)$$

where S_{stock} denotes the abundance (kg m^{-2}) of the corresponding element and fraction, C the concentration of the element in the corresponding fraction (kg t^{-1}), d_i the thickness of layer i (m), ρ_i = soil density (t m^{-3}) and RM the mass proportion of rock fragments/soil skeleton.

The analysis of the total elemental content in the fine earth (major and minor compounds) was done by means of X-ray fluorescence (XRF). Soil material (c. 5 g) was milled to < 60 μm and analysed as loose powder in sample cups using an energy dispersive X-ray fluorescence spectrometer (SPECTRO X-LAB 2000, SPECTRO Analytical Instruments, Germany).

3.2. Soil mineralogy

The clay fraction of the soils was obtained after removal of organic matter with diluted (3 %) and Na-acetate buffered H_2O_2 (pH 5) and then by dispersion with Calgon and sedimentation in water (Egli et al., 2001).

Orientated specimens on glass slides were analysed using a Rigaku SmartLab Automated Multipurpose X-ray Diffractometer equipped with a 3 kW sealed tube X-ray generator having a standard Cu target. Using Cu–Kα radiation generated at 40 kV and 30 mA, the slides were scanned in the range of 3–15° 2θ with a step of 0.01° 2θ and a speed of 2° 2θ per minute. Mg-saturation, ethylene glycol solvation (EG) and K-saturation were performed prior to X-ray diffraction (XRD) scanning. In addition, the K-saturated samples were heated for 2 h at 335 and 550 °C, and rescanned after each heating step. The XRD data of oriented specimens were corrected for Lorentz and polarisation factors (Moore and Reynolds, 1997) following Egli et al. (2001). Peak separation and profile analysis were carried out with Origin PFM™ following Lanson (1997) and Egli et al. (2001).

For quantitative X-ray diffraction analyses of the fine earth, randomly orientated (Zhang et al., 2003) Ca-exchanged samples were scanned from 4 to 80° 2θ using steps of 0.02° 2θ at 2 s intervals using a Bragg-Brentano X-ray diffractometer (Bruker AXS D8 Advance, Germany). The instrument worked with CoKα radiation that was generated at 35 kV and 40 mA and with dynamic beam optimisation (automatic theta compensating divergence slit and motorised anti-scatter screen). The diffractomter was equipped with primary and secondary soller slits, and an energy dispersive LynxEye XE-T line detector. Qualitative phase analysis was done with the software program DIFFRAC.EVA v4.3 (Bruker AXS). The minerals were identified by the positions and relative intensities of the peaks in the X-ray diffraction pattern compared with the PDF2 database (ICDD 1998). Quantitative mineral analyses were performed using Rietveld analysis of the XRD patterns and using the program Profex/BGMN V3.14.3 (Döbelin and Kleeberg, 2015).

3.3. Physical analyses: Grain size distribution and macropores

Prior to grain size analysis, 60 g of fine earth was dispersed in a 3% H_2O_2 solution to oxidise soil organic matter. The grain size distribution was determined using a procedure consisting of wet-sieving of the coarser particles (2000–32 μm) and X-ray granulometry (SediGraph 5100) measurements for the finer particles (32–1 μm).

Macropores freely drain water and are usually determined from soil pore size classes that were obtained from soil water retention curves (Amer et al., 2009). The use of these classes gave quite often rise to divergent results. Macropores and in general soil porosity are increasingly measured using X-ray CT and (macro)pores defined through the

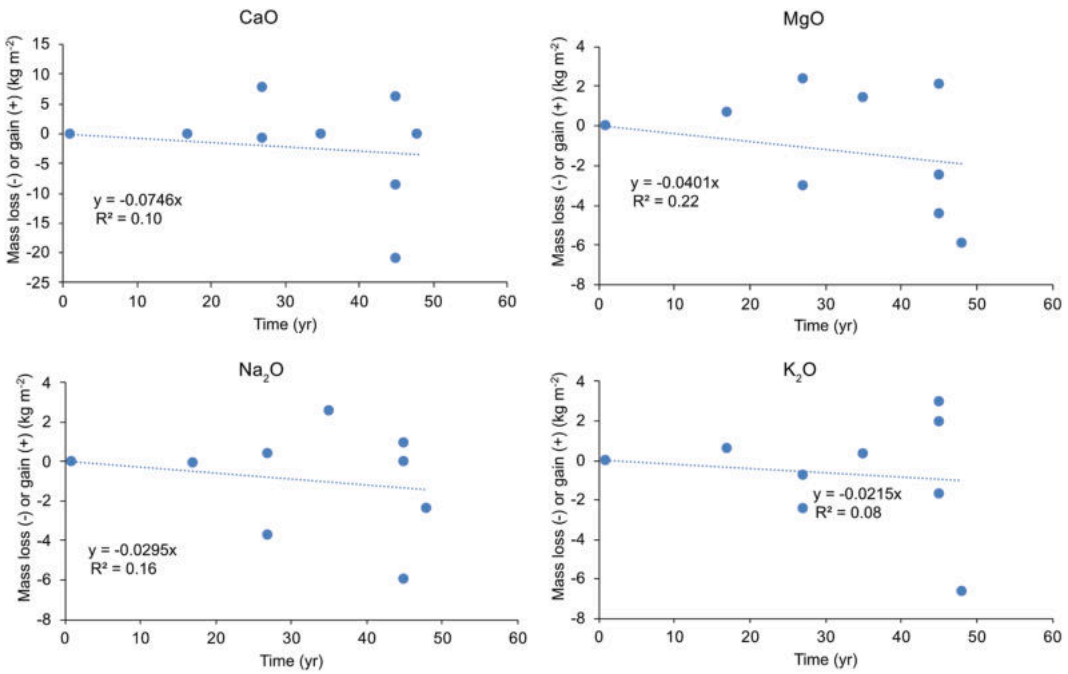

Fig. 6. Calculated mass losses (using Pb as immobile element) over time of CaO, MgO, Na_2O and K_2O.

Table 3
Calculated average element loss (Ca, Mg, Na) rates and accumulation rates of goethite (FeOOH) using three different immobile elements or compounds for the estimation of losses. Based on equation (5) (var 1) and 8 (var 2) two scenarios of CO_2 (mol m^{-2} yr^{-1}) and C (g m^{-2} yr^{-1}) consumption are calculated through the weathering of Ca, Mg and Na. According to Schroeder et al. (2000), each mole of FeOOH produced corresponds to about 2–3 moles of ∑(Ca, Mg, Na, K). K losses could not be detected in the investigated soils.

Immobile element/ compound	Element/ compound	Loss (mol m^{-2} yr^{-1})	CO_2 var 1 (mol m^{-2} yr^{-1})	CO_2 var 2 (mol m^{-2} yr^{-1})	C var 1 (g m^{-2} yr^{-1})	C var 2 (g m^{-2} yr^{-1})
Pb	Mg	0.99	0.99	1.98	11.9	23.8
	Ca	1.39	1.39	2.77	16.6	33.3
	K	0.47	0.47	0.47	5.7	5.7
	Na	0.79	0.79	0.79	9.5	9.5
	sum	3.64	3.64	6.02	43.7	72.2
Th	Mg	0.22	0.22	0.44	2.6	5.3
	Ca	2.77	2.77	5.55	33.3	66.6
	K	0.00	0.00	0.00	0.0	0.0
	Na	0.72	0.72	0.72	8.6	8.6
	sum	3.71	3.71	6.71	44.5	80.5
Non-carbonate	Mg	0.83	0.83	1.65	9.9	19.9
	Ca	4.36	4.36	8.72	52.3	104.6
	K	0.00	0.00	0.00	0.0	0.0
	Na	0.89	0.89	0.89	10.7	10.7
	sum	6.08	6.08	11.26	72.9	135.1
	FeOOH	0.78	1.55–2.33	3.10–4.65	18.8–27.9	37.2–55.8

pore diameters. The delimitations depend on the scan resolution and image processing (Luo et al., 2010).

Nine soil samples (100 cm^3; covering all ages of the sequence) were inspected using X-ray computational tomography (CT) using a GE Nanotom 180S device (GE Sensing & Inspection Technologies GmbH, Wunstorf, Germany). The samples were taken from the uppermost soil horizon (5), subsoil and/or parent material (4). The parameters of the X-ray source were the following: voltage – 130 kV, cathode current – 200 μA and a 0.2 mm Cu exit filter used to avoid beam hardening effect. The voxel size of the scan was 0.058 mm. During the scan, the samples were rotated through a full angle and at each of the 1800 angular positions a 2D view – averaged from 10 X-ray shots for noise reduction – of the sample were recorded. The next step after CT scanning was a 3D soil sample image reconstruction based on the recorded 2D radiograms. The reconstruction was done using the DatosX 2.0 software (GE Sensing & Inspection Technologies GmbH, Wunstorf, Germany). Finally, 16 bit grey-level 3D images of the scanned samples were generated. Subsequently, image analyses were done. Initially, from the whole 3D image of the soil core, the cylindrical region of interest (ROI) including only soil material was selected. The size of ROI was: 49.1 mm in diameter and 46.7 mm in height. The extracted ROI was then filtered three times by using a median filter having the smallest possible 3px kernel size. Thresholding was done using the IsoData algorithm (Ridler and Calvard, 1978) with thorough inspection of the thresholded images. After thresholding, the pore space of the soil samples was distinguished from soil material. The thresholded image of the soil material was then subjected to labelling, to distinguish between individual pores and skeleton analysis and to determine the pore network skeleton and its characteristics.

For the purpose of pores labelling, the group of voxels that are

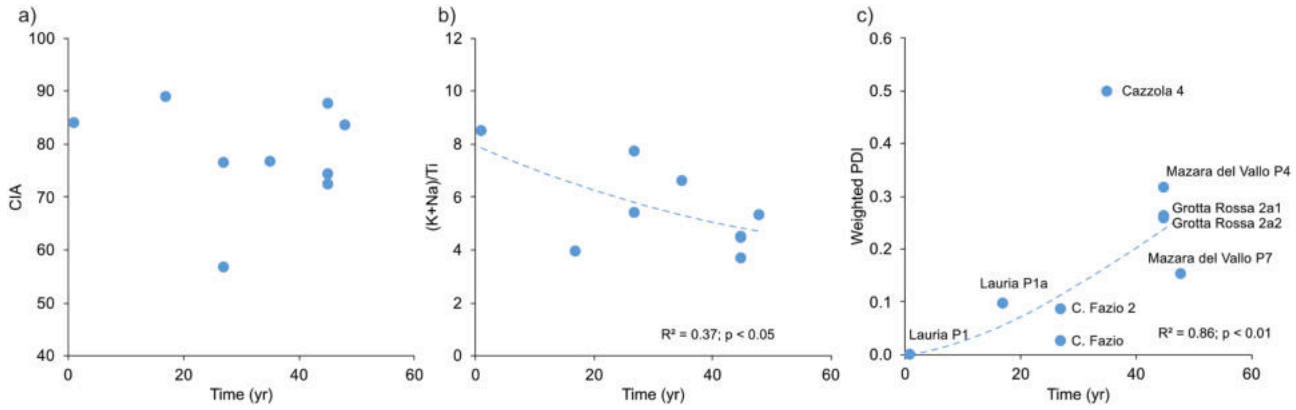

Fig. 7. Temporal trends of weathering indices (average value of A and B horizon), a) CIA, b) molar ratio of (K + Na)/Ti and c) weighted profile development index (PDI).

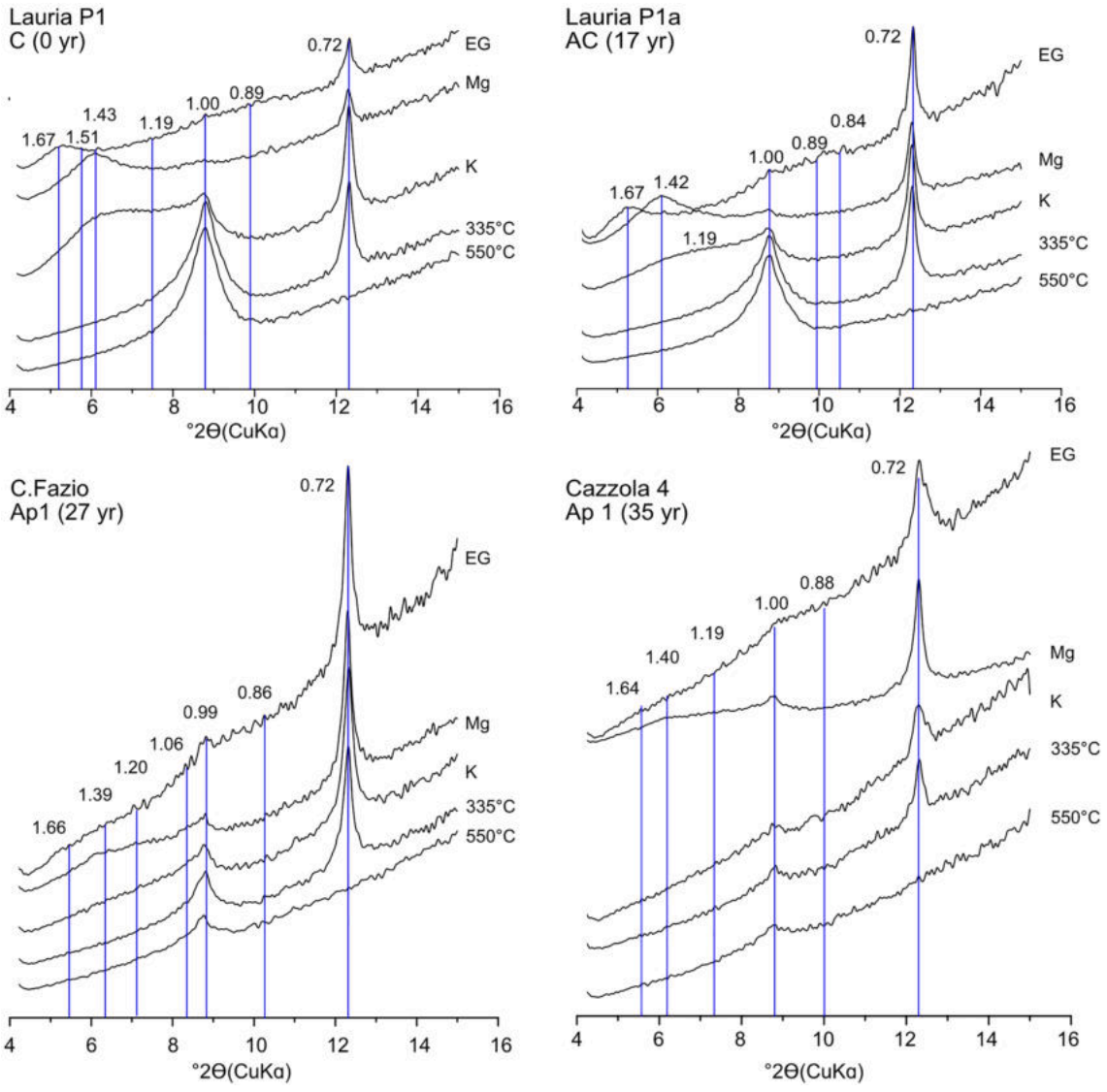

Fig. 8. X-ray diffractograms of several soil samples having a different exposure age. EG = ethylene glycol solvation, Mg = Mg-saturation, K = K-saturation, 335 °C and 550 °C = K-saturated and heated sample. The *d*-spacings are given in nm.

Table 4
Mineralogical composition of the fine earth.

Site	Horizon	Quartz	K-Feldspar	Na-Plagioclase	Aragonite	Calcite	Goethite	Rutile	Anatase	Kaolinite	Mica	Smectite	Chlorite
		wt.-%	wt.-%	wt.-%	wt.-%	wt.-%	wt.-%	wt.-%	wt.-%	wt.-%	wt.-%	wt.-%	wt.-%
1) Canicattì area													
Grotta Rossa 4a1	Ap	19.3 ± 0.02	3.9 ± 0.03	3.7 ± 0.01		12.1 ± 0.02	0.7 ± 0.02	0.5 ± 0.01	0.7 ± 0.01	6.6 ± 0.05	8.0 ± 0.04	43.0 ± 0.08	1.5 ± 0.02
	Bt	21.0 ± 0.02	5.5 ± 0.03	3.6 ± 0.01		3.4 ± 0.02	0.8 ± 0.02	0.5 ± 0.01	0.6 ± 0.01	6.8 ± 0.05	9.2 ± 0.04	44.9 ± 0.09	1.6 ± 0.02
Grotta Rossa 2a2	Ap	6.8 ± 0.02	2.1 ± 0.04	1.5 ± 0.01	1.0 ± 0.02	62.1 ± 0.04	0.4 ± 0.01		0.4 ± 0.01	2.0 ± 0.03	4.8 ± 0.04	17.9 ± 0.07	1.0 ± 0.02
	Ab	9.0 ± 0.02	2.1 ± 0.03	1.9 ± 0.01	1.1 ± 0.02	53.3 ± 0.04	0.5 ± 0.01		0.3 ± 0.01	2.9 ± 0.05	4.4 ± 0.05	23.4 ± 0.09	1.1 ± 0.02
Cazzola 4	Ap1	13.4 ± 0.02	3.3 ± 0.03	2.3 ± 0.01	0.7 ± 0.02	35.5 ± 0.02	0.4 ± 0.02	0.1 ± 0.01	0.5 ± 0.01	4.7 ± 0.05	6.8 ± 0.04	30.2 ± 0.09	2.1 ± 0.02
	Ap3	16.0 ± 0.03	2.7 ± 0.03	2.9 ± 0.01	0.2 ± 0.01	33.9 ± 0.02	0.1 ± 0.01	0.3 ± 0.01	0.6 ± 0.01	5.0 ± 0.04	6.8 ± 0.05	29.4 ± 0.08	1.6 ± 0.02
C.Fazio	Ap1	6.4 ± 0.02	1.8 ± 0.03	1.0 ± 0.02	0.6 ± 0.02	69.7 ± 0.04	0.3 ± 0.01		0.4 ± 0.01	3.0 ± 0.03	4.8 ± 0.04	11.2 ± 0.06	0.9 ± 0.02
	Ab	23.9 ± 0.03	3.5 ± 0.04	3.5 ± 0.02		10.0 ± 0.02	1.2 ± 0.02	0.4 ± 0.01	0.7 ± 0.01	10.8 ± 0.05	9.4 ± 0.05	33.9 ± 0.09	2.7 ± 0.02
C.Fazio 2	Ap1	12.1 ± 0.02	1.8 ± 0.03	1.5 ± 0.02		55.4 ± 0.05	0.5 ± 0.01		0.6 ± 0.01	4.8 ± 0.05	6.4 ± 0.05	15.7 ± 0.09	1.2 ± 0.02
	Ap3/Ab	14.6 ± 0.02	2.0 ± 0.03	1.6 ± 0.01		44.5 ± 0.03	0.6 ± 0.02		0.6 ± 0.01	7.7 ± 0.05	7.0 ± 0.05	20 ± 0.09	1.4 ± 0.02
Lauria P1a	AC	2.0 ± 0.01	0.5 ± 0.01	0.4 ± 0.01		89.2 ± 0.05				1.1 ± 0.04	1.5 ± 0.02	5.3 ± 0.05	
	C	0.7 ± 0.01				96.8 ± 0.02				0.2 ± 0.01		2.3 ± 0.03	
2) Mazara del Vallo area													
Mazara del Vallo Ferla	A	32.1 ± 0.04	5.1 ± 0.05	2.3 ± 0.02	0.8 ± 0.01	17.5 ± 0.02	1.3 ± 0.02	0.4 ± 0.01	0.8 ± 0.01	7.4 ± 0.05	5.4 ± 0.05	24.2 ± 0.11	2.5 ± 0.02
	C	0.9 ± 0.02			4.0 ± 0.02	90.4 ± 0.06				1.2 ± 0.05		1.9 ± 0.09	1.6 ± 0.02
Mazara del Vallo P7	Ap1	28.7 ± 0.03	4.0 ± 0.05	1.8 ± 0.02	0.5 ± 0.02	22.0 ± 0.02	1.0 ± 0.02	0.5 ± 0.01	0.9 ± 0.01	6.9 ± 0.05	5.3 ± 0.05	26.7 ± 0.09	1.7 ± 0.02
	C	21.1 ± 0.03	2.3 ± 0.05	2.0 ± 0.02	0.9 ± 0.02	33.6 ± 0.04	1.5 ± 0.02	0.3 ± 0.02	0.8 ± 0.01	7.0 ± 0.05	5.3 ± 0.07	23.2 ± 0.13	2.0 ± 0.02
Mazara del Vallo P4	Ap	8.7 ± 0.02	0.5 ± 0.02		1.4 ± 0.02	80.7 ± 0.07	0.6 ± 0.02		0.4 ± 0.01	1.6 ± 0.05	1.5 ± 0.05	2.6 ± 0.11	2.0 ± 0.02
	C	1.3 ± 0.02				98.0 ± 0.02	0.4 ± 0.02						0.3 ± 0.01

connected by at least one voxel face were treated as individual pores. Bigger pores were divided into sub-pores by cutting them automatically in the narrow area. Subsequently, the pore surface (as sum of external faces of pore voxels), pore volume (as sum of the voxel's volume) and the equivalent diameter (defined as the diameter of the ball having the same volume as the pore) of the pores were determined. Thresholded images were also subjected to the skeletonisation procedure. Technically skeletonisation consists of two steps: distance map creation (where the central areas of pores are determined) followed by thinning (which results in network creation). The final step is the analysis of the resulting pore network.

Image analysis tasks were performed using the software Fiji - ROI selection for filtering and thresholding (U.S. National Institutes of Health, Bethesda, MA, USA) and Avizo 9 for labelling and skeletonisation (FEI, Hillsboro, Oregon, USA).

3.4. Chemical weathering

To trace alteration processes in the soil, chemical weathering indices and a mass balance approach were applied. The CIA provides a quantitative measure of feldspar weathering (Nesbitt and Young, 1982; Buggle et al., 2011):

$$CIA = 100\left[\frac{Al_2O_3}{Al_2O_3 + CaO + Na_2O + K_2O}\right] \quad (2)$$

Furthermore, the molar ratio of (K + Na)/Ti was used as weathering index (Egli et al., 2020). In addition, the open-system mass transport function α (Chadwick et al., 1990; Egli and Fitze, 2000) was used. Relative elemental losses in the soil column were calculated using this function:

$$\tau = \left(\frac{C_{j,w} \bullet C_{i,p}}{C_{i,w} \bullet C_{j,p}}\right) - 1 \quad (3)$$

where: i denotes the immobile element, $C_{j,p}$ (g kg^{-1}) is the concentration of element j in the unweathered parent material, and $C_{j,w}$ is the concentration of element j in the weathered product (g kg^{-1}). Using the concept of immobile elements, absolute gains and losses (M) were calculated for n soil layers as:

$$M_{j,w}(\Delta z_w) = \sum_{a=1}^{n} C_{j,w}\left(\frac{\tau_{j,w}}{1+\tau_{j,w}}\right)\rho_w \Delta z_w \quad (4)$$

where $\tau_{j,w}$ corresponds to the mass transport function and Δz to the weathered equivalent of the columnar height. The 'classically'-used immobile elements such as Ti or Zr were replaced by other elements and compounds that are less affected by chemical variability (such as the non-carbonate fraction, Th in carbonates and Pb; see Egli and Fitze, 2001).

A further means to trace weathering is the profile development index (PDI; Harden, 1982). To determine the PDI of a profile a number of easily measurable parameters can be taken into consideration (Lybrand and Rasmussen, 2015; Sauer, 2017). We used: horizon thickness, profile depth, soil colour (dry, wet), grain size distribution, stickiness,

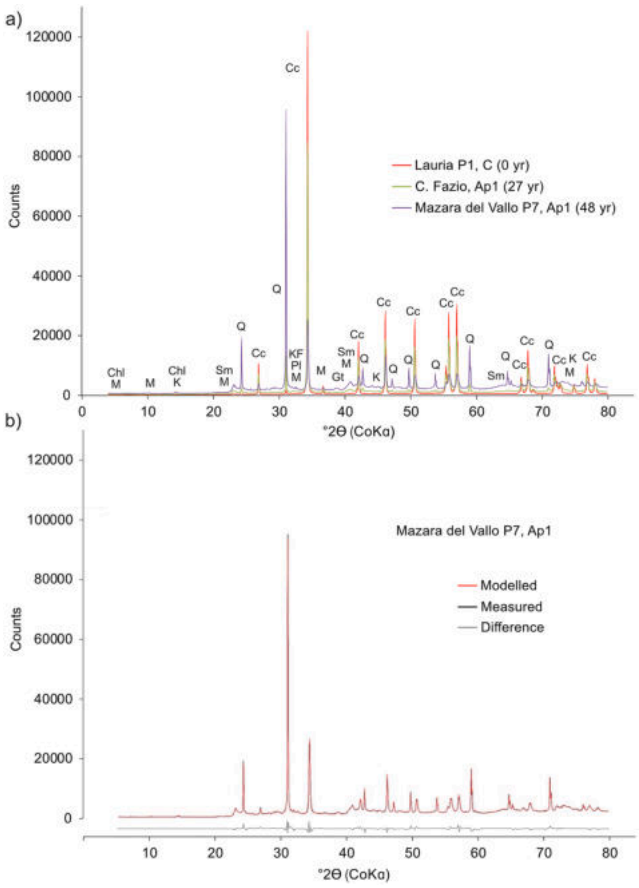

Fig. 9. a) X-ray diffractograms of soils having a different age. The diffraction peaks associated with calcite (Cc), quartz (Q), K-feldspar (KF), plagioclase (P), mica (M), smectite (Sm), kaolinite (K), chlorite (Chl) and goethite (Gt) are labelled. b) Rietveld plot of the sample Mazara del Vallo P7, Ap1.

plasticity, soil structure, consistency and the pH-value.

3.5. CO_2 consumption by silicate or carbonate weathering

With chemical weathering CO_2 is consumed. Urey (1952) proposed that atmospheric CO_2 combines with Ca silicates to produce carbonates. In the current literature an expanded version of the Urey reaction is given (Blättler and Higgins 2017; Kellogg et al., 2019). To include the role of acid rain the Urey reaction takes the form

$$CaSiO_3 + 2CO_2 + H_2O = CaCO_3 + SiO_2 + CO_2 + H_2O \quad (5)$$

The carbonation takes place when carbon dioxide (carbonic acid) dissolves calcium silicate (wollastonite) sediments to give calcium, bicarbonate, and silica (Kellogg et al., 2019).

Different procedures exist to calculate the CO_2 consumption by chemical weathering. Depending on the procedure, the results differ substantially. We used the approach of Hilley and Porder (2008) who assumed that each mole of Mg and Ca reacts with 1 mol of CO_2. In an extended form the consumption of CO_2 is described as:

$$CO_{2\ (sil)} = [Na^+]_{sil} + [K^+]_{sil} + [Ca^{2+}]_{sil} + [Mg^{2+}]_{sil} \quad (6)$$

with sil = silicate.

Another approach we applied follows Frondini et al. (2019) and Jiang et al. (2020). The alteration of anorthite and muscovite to kaolinite is described as

$$CaAl_2Si_2O_8 + 2CO_2 + 3H_2O = Al_2Si_2O_5(OH)_4 + 2HCO_3^- + Ca^{2+} \quad (7)$$

Table 5
Average oxalate-extractable contents of Fe, Al and Mn in the soils.

Site	Horizon	Depth	Al	Fe	Mn
1) Canicattì area					
Grotta Rossa 4a1	Ap	0–40	1358	857	424
	Bt	40–80	1954	812	415
Grotta Rossa 2a1	Ap	0–50	645	538	200
	AC	50–65	509	288	143
	C	65–75	193	193	56
Grotta Rossa 2a2	Ap	0–30	456	433	114
	Bw	30–85	523	413	160
	Ab	85–95	738	487	162
Cazzola 4	Ap1	0–40	850	604	456
	Ap2	40–80	747	555	430
	Ap3	80–100	599	540	383
C.Fazio	Ap1	0–50	235	555	168
	Ap2	50–75	397	1101	249
	Ab	75–85	418	1261	245
C.Fazio 2	Ap1	0–40	169	745	172
	Ap2	40–70	92	401	149
	Ap3/Ab	70–80	151	718	167
Lauria P1a	AC	0–30	138	135	73
	C	30–40	67	28	46
Lauria P1	C	0–10	59	13	15
2) Mazara del Vallo area					
Mazara del Vallo Ferla	A	0–20	1246	897	233
	C	20–40	1060	769	0
Mazara del Vallo P7	Ap1	0–20	366	292	62
	Ap2	20–75	69	29	288
	C	75–110	956	955	313
Mazara del Vallo P4	Ap	0–50	1507	791	342
	C	50–90	196	70	13

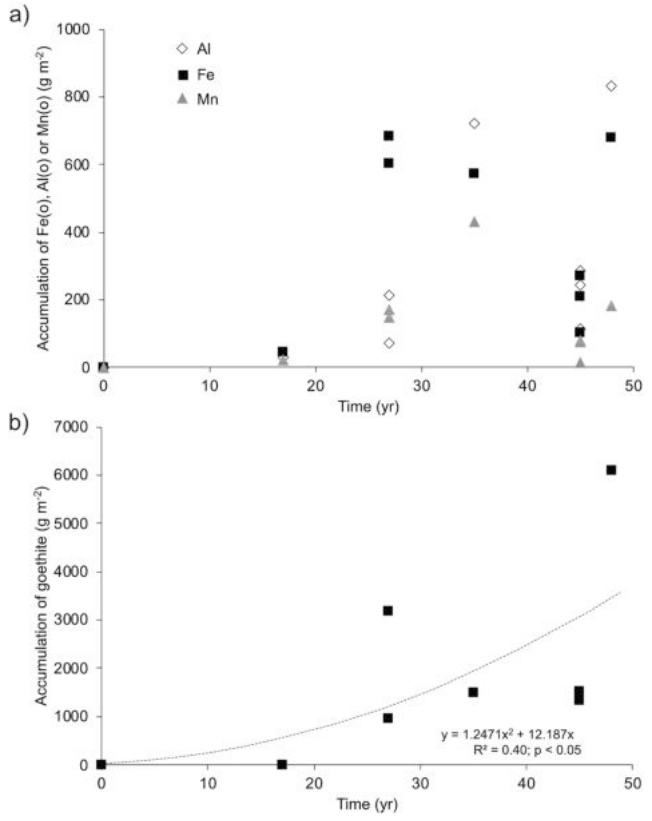

Fig. 10. Accumulation over time of a) oxyhydroxides (oxalate-extractable (o) contents of Fe, Al and Mn) and of b) goethite.

$$2KAl_2(Si_3Al)O_{10}(OH)_2 + 5H_2O + 2CO_2 = 3Al_2Si_2O_5(OH)_4 + 2K^+ + 2HCO_3^- \quad (8)$$

This means that per mol Ca, 2 mol of CO_2 are consumed and per mole K, 1 mol of CO_2. As a consequence, the overall consumption of CO_2 with silicate weathering is:

$$CO_{2\ (sil)} = [Na^+]_{sil} + [K^+]_{sil} + 2[Ca^{2+}]_{sil} + 2[Mg^{2+}]_{sil} \quad (9)$$

According to Frondini et al. (2019) and Jiang et al. (2020), also the dissolution of carbonates consumes atmospheric CO_2. The congruent dissolution of calcite follows:

$$CaCO_3 + H_2O + CO_2 = Ca^{2+} + 2HCO_3^- \quad (10)$$

Thus, the consumption of CO_2 due to carbonate weathering would be

$$CO_{2\ (carb)} = [Ca^{2+}]_{carb} + [Mg^{2+}]_{carb} \quad (11)$$

4. Results

4.1. General soil characteristics

All transformed sites have Anthrosols. The unaffected soils at Mazara del Vallo Ferla and Grotta Rossa 4a1 are a Regosol and Luvisol, respectively (Table 1). The thickness of the deposited unweathered and artificial layer on top of the former soil was at all sites relatively similar (approx. in the range of 80–100 cm; Table 2). Soil development on the most recently transformed sites was (Lauria P1a, Lauria P1), as expected, very weak. With time, a soil formation on the crushed limestone (that can be considered as new C horizon) started. The soil layer is mostly characterised by an Ap horizon; at some sites also a B (Grotta Rossa 2a2) or an AC (Lauria P1a) horizon developed. Soil thickness, defined as A and B horizon (transition horizons such as AC may count half; Sauer, 2010), steadily increases over time to attain a considerable average of about 70 cm after 45 years (Fig. 2). The skeleton content in the transformed soils varies considerably and reaches a maximum of >70 wt-% in C. Fazio 2 and Mazara del Vallo P4 (Table 2). This reflects that crushed rock material was added. With respect to the soil skeleton, no decrease with time could be detected. Because the rock material consists of crushed limestone, the carbonate content is high in all soils and consequently also the pH value.

The applied crushed rock material (after deposition and levelling) usually had a density in the range of 1.2–1.7 g cm^{-3} (Table 2). In general, soil bulk density decreases with time slightly probably due to the concomitant increase in organic matter (Table 2; Fig. 3). This trend is more obvious in the layer where a soil is developing. The C-horizon can be considered, in terms of soil evolution, as t = 0 because it reflects the original and unweathered state of the material. The LOI content, an indication for the organic matter content in the soil (Hoogsteen et al., 2015), increases distinctly during the first 20 years after soil amendment and then remains relatively constant in the soil with about 7 wt-% (Table 2). With increasing weathering and age of the soil material, the pH value decreases slightly, but still remains in a neutral to slightly-alkaline range (7.2–7.8). A strong negative relationship between LOI and pH was found ($R = 0.615$, $p < 0.05$), which is due to the H^+ dissociation from organic matter.

The soils cover a wide range of textural classes; i.e., from loamy sand to silty clay or clay (Table 2). The added crushed rock material is a relatively sandy limestone. With time, the proportion of clay (Fig. 3) and silt slightly increases and the sand content decreases. The Lauria and Mazara del Vallo profiles have the highest amount of sand (coming from the sandy limestone of the parent material) and the lowest amount of clay. The oldest transformed profiles at Mazara del Vallo and Grotta Rossa have a high silt content (up to almost 60%).

Table 6
Pore characteristics of the investigated samples (Canicattì area). The numbers related to a volume of 88.4 cm^3.

Site	Horizon	Age[1)] (yr)	Total pore volume (mm^3)	Max. graph length (mm)	Total macroporosity (%)	Total surface area of pores (mm^2)	Mean tortuosity	Max. graph number
Grotta Rossa 2a1	Ap	45	6174	61,522	7	61,320	1.16	100
Grotta Rossa 2a1	AC	17*	9785	108,737	11	94,557	1.13	50
Grotta Rossa 2a1	C	0	7381	65,318	8	62,280	1.15	89
Cazzola 4	Ap1	35	3469	46,521	4	34,618	1.13	39
C.Fazio	Ap1	27	7279	49,264	8	62,011	1.17	54
C.Fazio	Ab	–	1387	4137	2	7964	1.19	21
Lauria P1a	AC	17	8634	108,043	10	94,212	1.15	75
Lauria P1a	C	0	11,101	176,475	13	118,565	1.12	43
Lauria P1	C	0	7268	107,283	8	83,461	1.14	64

* Age interpolated.
[1)] Duration of weathering after site transformation.

Table 7
Organic carbon stocks of the transformed and natural soils of the region. The stocks are given for the entire soil profile and for 0 – 80 cm. The latter range is given, because the added artificial layer (crushed limestone), and thus the new soil, typically has this thickness. The basic data of the sites Tripoli1 – Gessi are form Egli et al. (2020). These sites are all near Canicatti (Fig. 1) and mostly have soils > 80 cm thickness.

Site	Parent material	Soil transformation	Land use	org. C stocks (total) kg m^{-2}	org. C stocks (0–80 cm) kg m^{-2}
Grotta Rossa 4a1	Limestone	No	Table grapes	15.07	15.07
Grotta Rossa 2a1	Limestone	Yes	Table grapes	3.81	3.45
Grotta Rossa 2a2	Limestone	Yes	Table grapes	7.98	7.75
Cazzola 4	Limestone	Yes	Table grapes	4.74	4.74
C.Fazio	Limestone	Yes	Table grapes	7.77	7.77
C.Fazio 2	Limestone	Yes	Table grapes	3.46	3.46
Lauria P1a	Limestone	Yes	Table grapes	1.15	1.15
Lauria P1	Limestone	Yes	Table grapes	0.00	0.00
Mazara del Vallo Ferla	Limestone	No	Pasture	8.58	8.58
Mazara del Vallo P7	Limestone	Yes	Table grapes	11.37	9.28
Mazara del Vallo P4	Limestone	Yes	Table grapes	7.48	7.48
Tripoli 1	Laminated marl (diatomite)	No	Uncultivated area	19.91	13.65
Tripoli 2	Laminated marl (diatomite)	No	Uncultivated area	38.88	14.87
Detriti	Limestone	No	Vineyard	31.89	18.25
Calcare	Limestone	No	Pasture	28.30	28.30
Argille 5	Clays and marl	No	Pasture	12.92	10.58
Argille 6	Clays and marl	No	Fruit orchard	7.96	5.74
Argille 7	Crushed limestone over clays and marl	Yes	Vineyard	26.54	19.88
Gessi	Gypsum	No	Pine forest	11.70	11.70

Average stocks in old (not transformed) soils on limestone: 22.1 kg m^{-2} (±9.3; whole soil), 18.3 kg C m^{-2} (±7.2; 0–80 cm).

4.2. Inorganic and organic carbon

The transformed soils Lauria P1 and P1a and Mazara del Vallo P4 contain the highest amount of total carbon (bound in carbonates), while the oldest transformed soils (Mazara del Vallo P7) exhibits the lowest (Table 2). In general, the carbonate content is quite high throughout all soil profiles due to the carbonate-rich material that was added. The C-horizons typically contain the highest carbonate concentrations; but, also some horizons near the surface (C. Fazio Ap1) contain up to 57 wt-% of $CaCO_3$. The quite homogeneous carbonate depth distribution can be explained by the mixing of the material during the construction. Organic C distinctly decreases with depth in most of the transformed soils. The oldest transformed soils contain the highest organic C content.

The organic carbon stocks increase rapidly and significantly with time (Fig. 4). The maximum org. C stock is reached in the oldest transformed soil with 11.4 kg m^{-2} (Mazara del Vallo P7). This stock is considerably high. The org. C stocks seem to increase linearly with time. However, such a trend does not follow normal pedogenesis and cannot be extrapolated tel quel. With time, a quasi-steady state stock must be reached. Unaffected agricultural and natural soils of this region have a stock that varies within a wide range (Novara et al., 2017) and can be, if the A and B horizons are considered, even very high (>40 g org. C m^{-2}; Scalenghe et al., 2015; Egli et al., 2020). One usually surmises that a quasi-state situation is reached with time (Egli et al., 2012). Logistic functions that trace soil organic carbon stocks as a function of time and having different asymptotic end-values are plotted in Fig. 5. It is also interesting to note that the Regosol has, although being relatively shallow, a high organic carbon stock with 8.6 kg m^{-2}. In a similar range is the untransformed soil Grotta Rossa 4a1 with an org. C stock of 15.1 kg m^{-2} (Table 7). The average sequestration rates of org. C of the investigated transformed soils vary between 68 and 288 g m^{-2} yr^{-1}. Assuming a logistic function, the rates would remain high until about 50–100 years since start of the soil transformation and would strongly decrease thereafter (Fig. 5).

Using the isotopic composition of the carbonates measured in the soils and the endmembers -$\delta^{13}C$ = −1‰ for carbonates and –23.8‰ for biogenic matter (Egli et al., 2020) of the region – the proportion of pedogenic carbonates was estimated. This proportion steadily increases with increasing age of the artificial soils pointing to the dissolution and reprecipitation of carbonates or to chemical weathering of primary silicates (Table 2). The proportion of secondary carbonates on total inorganic carbon reaches about 50% at the site Grotta Rossa 4a1.

4.3. Chemical weathering

All samples contain carbonates; in some cases, up to >90 % (Lauria P1, Lauria P1a, Mazara del Vallo P4; Table 2). Due to the high carbonate content and related dilution effect, particularly Zr exhibited partially very low contents and showed a high variability along the profiles (Table S1). When using them as immobile elements it resulted in unrealistic chemical weathering losses or gains (Eq. (4)). Therefore, Th was additionally used as an immobile element because it occurs in insoluble form also in carbonates (Bailey and Ragnarsdottir, 1994). A further immobile element in such environments is Pb.

Only a slight weathering of silicates is detectable with time (Fig. 6). Weathering of silicate components (CaO, Na_2O, K_2O, MgO) is dominated by CaO and, to a lesser extent, by Na_2O. The highest CaO + Na_2O + K_2O + MgO (silicate compounds) leaching was found at the site Mazara del Vallo P4 (Fig. 6). The average weathering rate of silicate compounds was, depending on the calculation scenario, about 170–280 g m^{-2} yr^{-1} (or about 3.7–5.5 mol m^{-2} yr^{-1}, Table 3). It was not possible to detect a significant loss of carbonates over the considered time span of approx. 50 years seem, because primary carbonates were dissolved, moved and re-crystallised as pedogenic carbonates. In general, changes and weathering losses are difficult to recognise during the first 30 years of weathering and soil formation. Thereafter, it seems, however, that silicate weathering becomes more evident (Figs. 6 and 7).

With time the molar ratio of (K + Na)/Ti tends to decrease pointing to increasing weathering conditions (Fig. 7). This decrease might be partially linear, but would not be plausible in the long-term. The CIA-values shows no trend. The most distinct changes over time, indicating weathering, can be seen with the PDI (Fig. 7). The values significantly and distinctly increase over time indicating that profile development and weathering indeed occurs. The observational period is short. Also here, the trend is not linear and would follow most likely an exponential decay model with an asymptotic value.

4.4. Soil and clay minerals

The samples of the youngest site and the original material used for soil transformation exhibit major peaks at the positions of 0.72, 1.0 and 1.43 nm in the textured XRD patter of the clay fraction. With ethylene glycol saturation, the peak centred at 1.43 nm moves to 1.67 nm, indicating the presence of smectite (Fig. 8; particularly well pronounced at Lauria P1 and Lauria P1a). As no primary chlorite can be traced in the

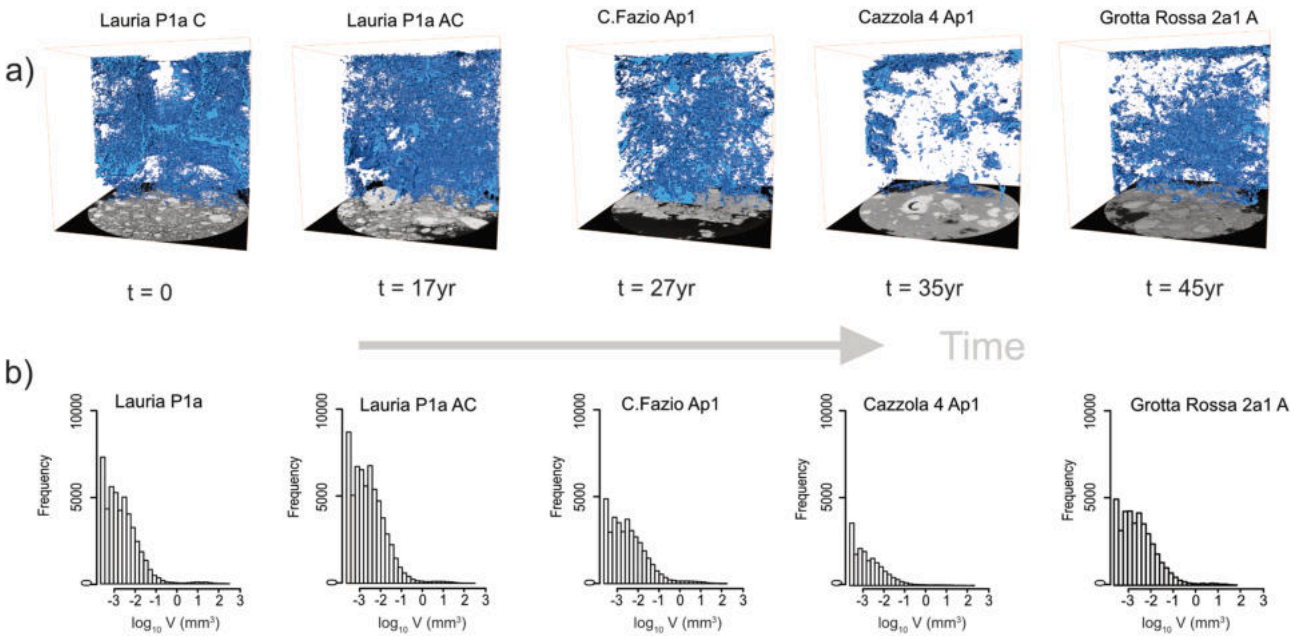

Fig. 11. a) Visualisation of the macropores (voxel size > 0.058 mm) and their evolution over time obtained from microtomographic scanning, b) frequency distribution of the pore volumes.

clay fraction, the peak at 0.72 nm indicates kaolinite. With K-saturation, the relative proportion of the peak at 1.00 nm increases. Consequently, also some vermiculite is present in the samples. A part of the peak at around 1.43 nm resists to K-saturation but collapses with heating at 335 °C to 1.00 nm. Therefore, some hydroxy-interlayered smectite or vermiculite is present (HIS or HIV). This general pattern remains more or less unaffected over time (except that the increasing content of hydroxides starts to disturb the XRD pattern). More interstratified minerals (mica/vermiculite or mica/HIV) start to develop over time, indicated by an increasing proportion of peaks between 1.00 and 1.43 nm; mostly near 1.24 nm; Fig. 8; C. Fazio and Cazzola 4).

The total mineral fraction revealed that calcite is, not surprisingly, the most abundant mineral in the measured profiles (3–98 wt-%) followed by quartz and smectite (Table 4, Fig. 9). Mica, kaolinite, K-feldspar and plagioclase were detected in all soils. In most samples, also some goethite could be measured. The measured X-ray diffractogram patterns could be best modelled (Fig. 9) using the minerals given in Table 4. With time, the content of calcite is decreasing giving rise to a relative increase of all other minerals. If the relative content of all non-carbonate minerals is considered, then a significant decrease in mica and a trend to a slight decrease in plagioclase and smectite can be figured out. At the same, chloritic compounds (e.g., HIV) increase. This indicates that some weathering of primary silicates is taking place.

The content and stocks of oxalate-extractable Al, Fe and Mn (Table 5), and thus weakly and poorly crystalline weathering products, distinctly increase over time (Fig. 10). Furthermore, also the amount of goethite significantly increases over time. This again supports the finding that active weathering occurs at a relatively high rate.

4.5. Evolution of macropores

The macro-porosity was in the range of 1.5 to about 13 % of the total volume. In general, these are rather low values. Usually, the C- or AC-horizons, and thus the added crushed material, have a higher macro-porosity than the A or Ap horizons (Table 6). Although the number of observations is low, it seems that the macro-porosity in the topsoil decreases with time after soil transformation (Fig. 11). The total surface area of the macropores was higher in the C and AC horizons compared to the A or Ap horizons (Table 6).

The pore length (maximum graph length) of the macropores normally decreased from the C and AC horizons to the A and Ap horizons and, thus, also with time (Table 6; Lauria P1a, Grotta Rossa 2a1). The temporal trend of the macro-porosity and pore length of macropores indicates that over time the volume of larger pores was reduced. It appears however that the tortuosity slightly increased from the C to the A horizons and thus also with time.

The pore graph represents the topology of the pore space (Table 6; Musso et al., 2019). Its edges connect the pores and store the diameter of the largest particle that can move along this edge (Mehlhorn et al., 2009). The number of pore networks slightly increases from the C to the A horizon whereas the graph length significantly decreases with time and from the C to the A horizons (Table 6). This indicates that the more networks appear, the shorter they are. Consequently, with time the porosity (Fig. 12), pore surface and pore length are reduced (Table 6). Something similar seems to happen with the temporal evolution of the pores and related network. With time, both bulk density (due to the increase in organic carbon content; Fig. 3) and – rather unusually – the proportion of macropores decreases. Simultaneously, the pore length (max. graph length) of the macropores decreases. A lower bulk density with time means therefore that less macropores are present. The remaining macropores have furthermore a shorter pore length (Fig. 12). With time, more organic matter is incorporated in the soil that probably gives rise to the disruption of the macropore length.

5. Discussion

5.1. Inorganic C

The $\delta^{18}O$ values of carbonate vary between −5.8 and + 0.2 ‰ (Fig. 13a). These values principally suggest that the carbonate has been formed in an ocean regularly influenced by freshwater (Oehlert and Swart, 2014; Caruso et al., 2015; Egli et al., 2020). However, during weathering, rainwater additionally impacts the $\delta^{18}O$ composition of particularly secondary carbonates (Egli et al., 2020) and drives the signal to more negative values. The present-day rainwater composition in Sicily has for an altitude of 100–300 m a.s.l. a $\delta^{18}O$ of about −6.2 to −6.4‰ (Liotta et al., 2013). The $\delta^{13}C$ value of marine carbonate should be typically near zero. With an increasing carbonate content, also the

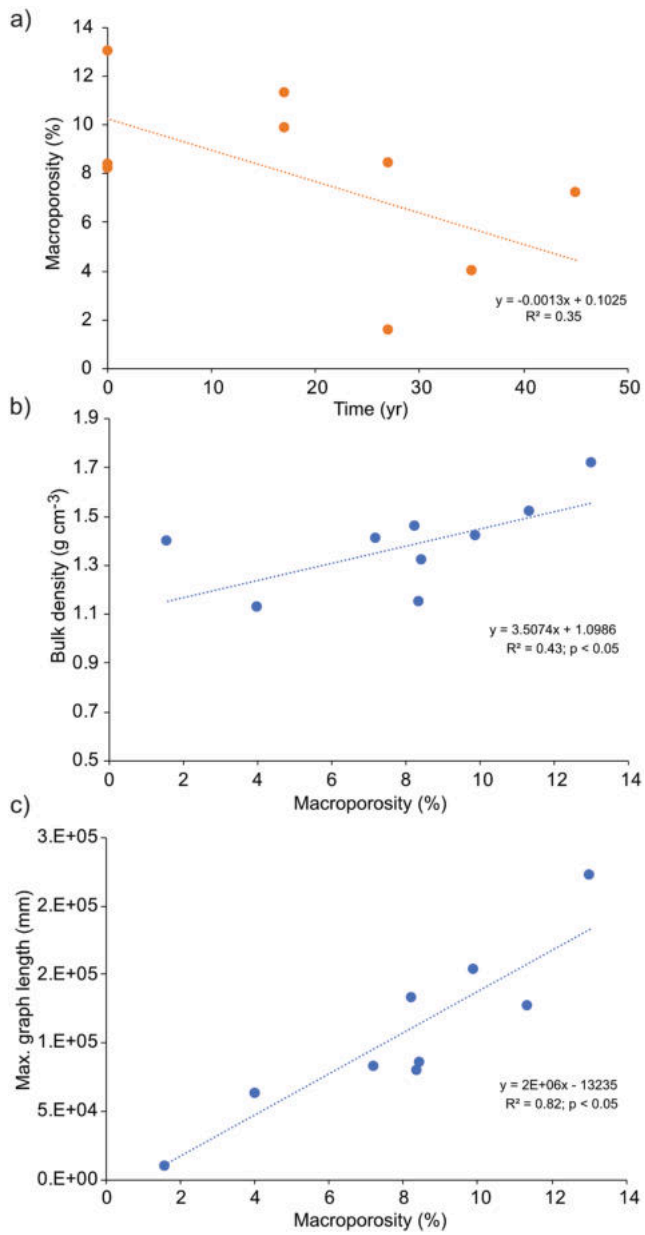

Fig. 12. a) Evolution of the macroporosity in the transformed soils. The macroporosity significantly decreases with time. Relation of the macroporosity with b) bulk density and c) max. graph length (pore length).

$\delta^{13}C$ values in the carbonates (overall signal of the marine and pedogenic carbonates) themselves and bulk soil (mixed signal between organic and inorganic carbon) become less negative (Fig. 13b,c). This is reflected in the positive relationship between the $CaCO_3$ content and $\delta^{13}C$ of both bulk soil and carbonates. The variability of $\delta^{13}C$ at high carbonate contents is much less compared to low carbonate contents. This means that a distinct part of the $CaCO_3$ was dissolved and reprecipitated (secondary carbonates) having the imprint of respired CO_2-C from the vegetation. As previously shown, the proportion of secondary carbonates on the total carbonate content increased continuously with the age of the soils. Under arid to semi-humid climatic conditions, dissolution of primary carbonate and recrystallisation with carbon (C) from soil CO_2 leads to the accumulation of significant amounts of pedogenic (secondary) carbonate (Gocke et al., 2012). In addition, the pedogenic carbonate slightly increased with increasing soil depth. This is probably due to leaching from the upper part followed by a reprecipitation in the lower part of the soil.

Typically, the $\delta^{13}C$ ratio of the bulk soil tends to more negative values with an increasing organic carbon content (Fig. 13d,e; Egli et al., 2020; Khedim et al., 2020) owing to the vegetation and its corresponding organic decay products having a different isotopic C signal.

5.2. Organic C and sequestration

The sequestration rates of organic C of the investigated transformed soils are very high with 68 and 288 g m^{-2} yr^{-1} and comparable to or even higher than very young alpine, natural soils that are known to be very reactive. In such soils, the rates were in the range of 3 to about 100 g C m^{-2} yr^{-1} (Egli et al., 2012). Consequently, the accumulation and sequestration of organic C in the transformed Mediterranean soils proceeds very quickly. Similar to young (alpine) soils, the C accumulation rates of transformed soils are high at the beginning and tend to reach a quasi-steady state after about 100–200 years (Fig. 5). The temporal trend of the accumulation rates also depends on the asymptotic end value. Usually, the thickness of the added layer of crushed limestone rocks comprises about 80 cm. A comparison with untransformed but agriculturally used soils on limestone shows that in average about 15 kg C m^{-2} can be stored in the layer 0–80 cm (Table 7). The temporal trends of organic C accumulation rates seem therefore most likely for model 1 and 2 (Fig. 5) where an asymptote in the range of 11 to about 18 kg m^{-2} and transformed soil thickness of 80 cm is reached. In general, these soils are capable to store a high amount of organic C in the entire, often deep profile (26–39 kg org. C m^{-2}, Table 7). Some of these natural profiles may have a thickness of >270 cm and still contain organic C in that depth (Egli et al., 2020). Although a high amount of sequestered C is often stored in the topsoil, the subsoil contained a substantial stock. Usually, the topsoil has a higher proportion of the labile organic C pool which is frequently replaced by new organic matter or respired (Jackson et al., 2017). For a long-term sequestration, organic C should also be stored in the subsoil (Luo et al., 2010; Aguilera et al., 2013; Angst et al., 2018; Laban et al., 2018).

The organic C sequestration potential in transformed Mediterranean soils thus seems, provided with good agricultural practice, enormous. While the observed time span seems to be too small to see distinct effects of silicate weathering, the carbon sequestration rates are considered to be high (Vicente-Vicente et al., 2016), because they tend to be very fast during the first years after a change of the management and progressively slow down. Aguilera et al. (2013) report very high sequestration rates of C in soils under organic amendment treatments with 144 g m^{-2} yr^{-1} or 27 g m^{-2} yr^{-1} in cover crops in Mediterranean areas. Novara et al. (2017) found that the abandonment of cropland in the Mediterranean leads to an increase in the soil organic carbon stocks by an average of 9.03 Mg C ha^{-1} in 20 years (=45 g m^{-2} yr^{-1}). Other studies from the Mediterranean region showed similar or far lower carbon sequestration rates with 0 to 46 g m^{-2} yr^{-1} (Álvaro-Fuentes et al., 2009). In a 50-yr field experiment with soils having initially no organic C, Kauer et al. (2019) measured organic C accumulation rates, depending on the type of cultivation, of 11–50 org. C m^{-2} yr^{-1}. The values we measured are very high, also because we did not only look at the carbon accumulation in the topsoil, but considered the whole profile. Over a period of maybe 50–100 years, the goals of the '4 per mille' initiative can be easily achieved in areas where soils are transformed. Minasny et al. (2017) come to a similar conclusion. Based on an investigation and data evaluation of 20 regions in the world, high C sequestration rates (up to 10 per mille) can be achieved for soils with low initial SOC stocks (topsoil <3 kg C m^{-2}) and at the first twenty years after implementation of best management practices (reduced tillage in combination with legume cover crops). Other authors (Valkama et al., 2020) showed that the type of land use is crucial if the goal of the '4 per 1000' initiative can be reached or not. According to these authors there is in principle no alternative solution to that of conservation agriculture. However, the extent to which organic C is stored depends on the soil type, its characteristics and climate.

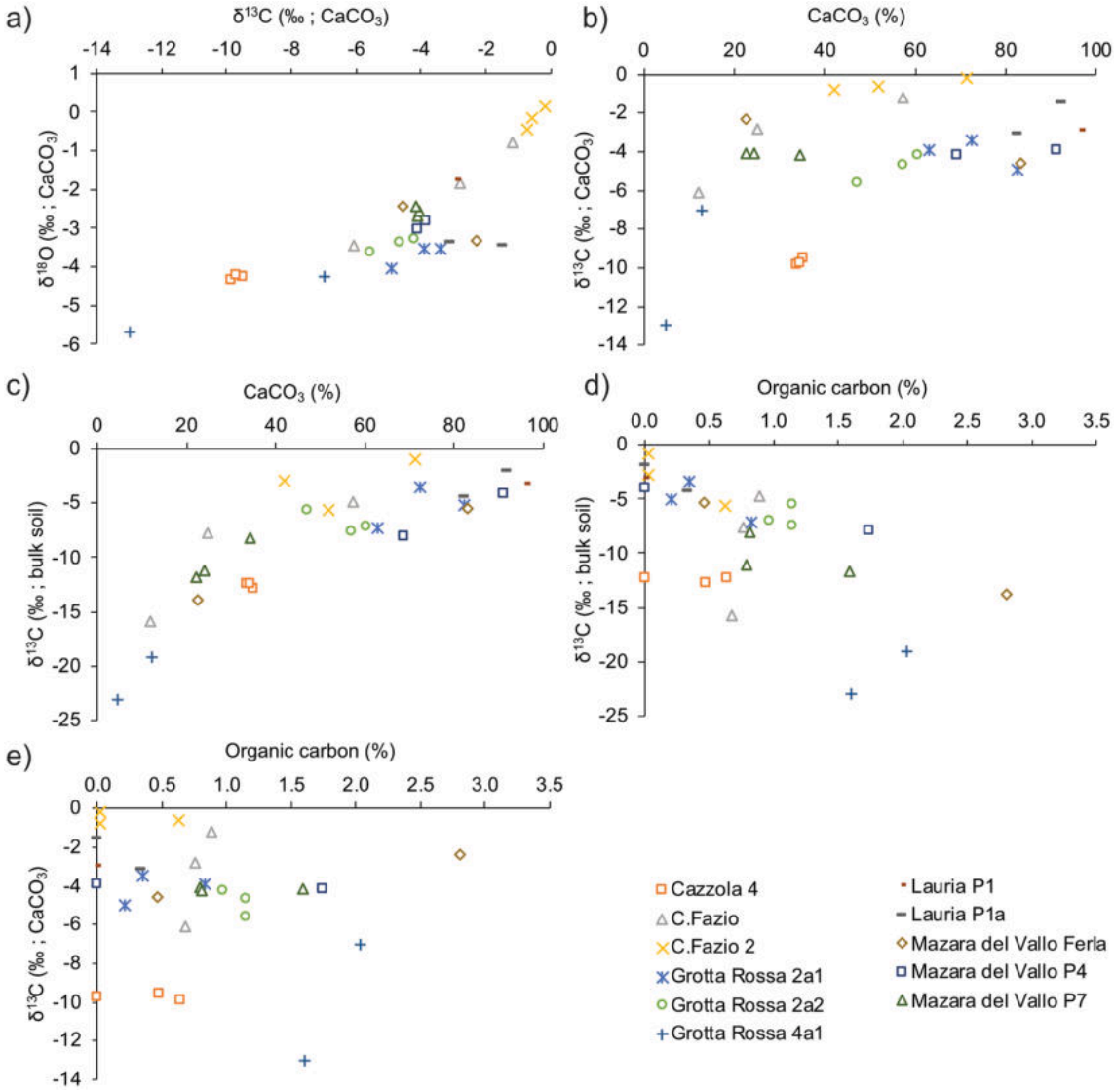

Fig. 13. Comparison between a) $\delta^{13}C$ ratio and $\delta^{18}O$ ratio of the carbonates, b) the carbonate content and the $\delta^{13}C$ ratio of the carbonates, c) the carbonate content with the $\delta^{13}C$ ratio of the bulk soils, d) organic carbon content of the bulk soil with the $\delta^{13}C$ ratio of the bulk soils and e) organic carbon content of the bulk soil with the $\delta^{13}C$ ratio of the carbonates.

5.3. Chemical weathering and C consumption

The PDI is one of the most widely-used soil development index based on field and laboratory data (Sauer, 2017). This index has been applied on a wide range of environments. The PDI distinctly increases with soil age indicating fast weathering processes. Compared to soil chronosequences of other sites having a Mediterranean type of climate (e.g., California; Busacca, 1987; McFadden and Weldon, 1987) or glacial deposits of alpine regions (Goodman et al., 2001; Dahms, 2002), similar values were calculated for soils having an age of several kyr. At our investigated sites, however, high values are reached much earlier.

Other chemical weathering indices are less sensitive. The CIA and particularly the (K + Na)/Ti ratio indicate some modest weathering, however by far not so clear as one can usually detect on long-term observations (Sauer et al., 2010).

Silicate weathering is difficult to be correctly quantified over the considered time span (Fig. 6). The losses or gains are small. Depending on the immobile element used for the calculation of gains or losses, about 5.8–12.5 kg $\sum$(CaO, Na_2O, K_2O, MgO) m^{-2} were leached in 45 years. The average leaching rates (although the variability is large and the time trends are not so clear and only for CaO statistically significant) were estimated to about 3.5–10 kg m^{-2} for CaO, 0.5–1.4 kg m^{-2} for MgO, 0.9–1.25 kg m^{-2} for Na_2O and 0–1.7 kg m^{-2} for K_2O in 45 years (Table 3; Fig. 6). These trends might have been affected by the fact that some sites had a higher slope angle causing some erosion (although no visible erosional features were detectable) which influences chemical weathering (Hilley and Porder, 2008). In terms of consumed atmospheric C due to weathering, the rates are between 44 and 73 (based on equation (6)) and 72–135 g C m^{-2} yr^{-1} (based on equation (9); Table 3). These results are surprising: the rates of atmospheric C consumption by chemical weathering do not seem to be that much lower than the sequestration of organic C. However, we must clearly note that these calculations are bound to relatively large uncertainties. With time, we see a distinct accumulation of newly formed goethite (Fig. 10). Goethite is a weathering product and normally derives from the weathering of hornblende, epidote and/or biotite. With the formation of FeOOH no CO_2 is directly sequestered. However, when hornblende, epidote and/or biotite weather, they release not only Fe but also Ca, Mg, K and Na. Therefore, the formation of FeOOH may be an indicator of the release of Ca, Mg, K and Na and thus CO_2 consumption with weathering. According to Schroeder et al. (2000), each mole of Fe that is released from primary minerals (biotite, hornblende, epidote) corresponds to about

2–3 mol of ∑(Ca, Na, K, Mg). The formation rate of goethite can therefore be used as a cross-check of silicate weathering and CO_2 consumption (Table 3). Although the average leaching rates of Ca, Na, K, Mg are bound to a high uncertainty, they correlate very well with the values estimated by using FeOOH. This cross-check shows that the calculated CO_2 consumption rates by silicate weathering might therefore be in a reasonable range. It seems (see chapter 5.4) that mica weathering is one of the most important processes. Biotite often is the primary source of Fe incorporation into secondary goethite (White et al., 2017).

According to the equations (10) and (11) carbonate dissolution also contributes to the consumption of atmospheric CO_2 (Frondini et al., 2019; Jiang et al., 2020). Over 45 years, about 200–400 kg $CaCO_3$ m^{-2} would have been leached. This would be enormous. In terms of C consumption this would give rise to a rate of about 500 to about 1000 g m^{-2} yr^{-1}. This does not seem to be realistic (particularly the highest value). In addition, dissolved carbonates do not remain eternally in the groundwater. Sooner or later, they precipitate and the process will be reversed. It is therefore questionable if the dissolution of carbonates really contributes to atmospheric CO_2 consumption.

The high C consumption values calculated when using equation (9) for silicate weathering and the carbonate weathering do not take into account that CO_2 is only temporarily stored as HCO_3^- in the soil and groundwater because it will degas later. Thus, the calculated silicate weathering and CO_2 consumption using equation (6) gives more plausible results. This means that atmospheric carbon is consumed at a rate of 44–72 g C m^{-2} yr^{-1}.

The amount of oxalate-extractable Al, Fe and Mn increased distinctly with time. The oxalate-extractable contents are about 30–50% lower when compared to non-transformed and well-developed soils of the region (Egli et al., 2020). However, soil formation and pedogenic transformations are still ongoing at high rates. Fe and particularly Al correlated significantly ($R^2 = 0.28$ and 0.53, respectively; $p < 0.05$) with the organic matter content. It is commonly known that oxyhydroxides can bind strongly organic matter (Wiesmeier et al., 2019).

Such high chemical weathering and transformation rates do not exist in natural soils of this region. Agricultural use and related irrigation accelerated these processes.

5.4. Soil and clay minerals

The undisturbed and, thus, oldest soils have a lower calcite content in the A and B horizon than the transformed sites (Table 4). Although the variability is relatively large, the calcite content in the topsoil generally decreased with time ($R^2 = 0.51$; $p < 0.05$). As a concomitant effect (normalised to 100%), the other minerals are passively enriched (Table 4). Mica seems to decrease whereas chlorite components increase over time. With weathering, mica can be transformed to HIV or HIS (both having the characteristics of chloritic components; Ezzaïm et al., 1999; Tolpeshta and Sokolova, 2018). Over time, more interstratified minerals were formed indicating an active weathering environment (e.g., Carnicelli et al., 1997). Most of the detected (clay) minerals must therefore originate from the crushed rock material and do not change greatly in their relative proportion.

The amount of goethite increases distinctly over time (Fig. 10). In soils, hematite and goethite are usually formed in the presence of clay minerals or primary minerals. Their formation pathway however can be complex (Schwertmann et al., 2000; Wilson, 2004).

5.5. Macropores

The rather sandy soil (high carbonate content) at the start of the soil evolution suggests that the soil pores have a comparably large soil pore volume (macroporosity) (Singh et al., 2018). Sandy soils have however only a small relevance in protecting SOC from mineralisation because of the lack of smaller pore sizes stabilising organic material (Chivenge et al., 2007). The distribution of soil pores therefore influences the soil organic carbon cycle. Likewise, as particles usually decrease in size due to weathering (Taylor et al., 2017), the pore size distribution and water permeability also change (Andrews and Taylor, 2019). Hirmas et al. (2018) mentioned that macropores often represent <1 % of the soil volume, but can contribute to >70 % of the total soil water infiltration.

The macroporosity of the investigated soils significantly decreased over time. Similar to results of Musso et al. (2019), the number of small pore volumes increased and the relative proportion of large pore volumes decreased with time (Fig. 11). The macroporosity is at the beginning of the soil transformation (after addition of the crushed material) about 10% and after 45 years only half of it, i.e., about 5 % (Fig. 12). These volumes (based on a similar or moderately similar voxel size), are often measured in agricultural or natural soils (Kochiieru et al., 2018; Yang et al., 2018).

In terms of organic carbon conservation, the investigated soils develop in a favourable direction. The development of macropores is finally dependent on several factors such as SOC content, grain size distribution (Nemes et al., 2005), agricultural techniques (ploughing, heavy machinery, etc) and soil biology (Jarvis, 2007). Macroporosity and the max. graph length indeed correlate positively ($R^2 = 0.82$; $p < 0.05$; Fig. 12), indicating that macropores tend to extend the soil pore network. With a decrease in macroporosity, macropore length is shorter (Fig. 12). Together with a smaller proportion of macropores and smaller lengths, meso- and microporosity is hypothesised to increase (no data available) giving rise to a better water retention. This can be beneficial for plants; however, with a too high water supply the contrary will happen owing to the development of redoximorph conditions.

The sandy limestone material had, according to the information of the local farmer and according to Crescimanno et al. (1987), Lombardo and Raimondi (1991) and Raimondi and Sarno (1999) a positive influence on the grape quality. The presence of carbonates renders the peel of the grapes more crispy and more resistant for the transport to the European market. The addition of sandy limestone, however, also bears the risk that calcretes may form deeper in the profile affecting the water infiltration and penetration of roots (Wright and Tucker, 1991). The challenge now remains in maintaining the favourable soil properties in order to keep the positive influence.

If these soil transformations are not well done, they could trigger deterioration of both soil ecosystem services and environmental quality (Dazzi et al., 2019).

6. Conclusion

Transformed soils containing crushed carbonates seem to have a huge potential for absorbing and sequestering organic carbon from the atmosphere. By using a chronosequence (from 0 to 48 years), soil changes since the surface transformation could be quantified with respect to atmospheric CO_2 consumption. Irrigated and transformed soils that are used for table grapes showed organic carbon sequestration rates in the range of 68 to 288 g m^{-2} yr^{-1}. As a consequence, up to about 12 kg C m^{-2} could be stored in the soils since transformation. Chemical weathering proceeded fast with the formation of soils exhibiting well developed horizons. The profile development index traced the development well. Within 48 years, a substantial amount of carbonate was weathered and in part transformed into secondary carbonates. Because carbonate weathering consumes in a first step atmospheric CO_2 and releases it after reprecipitation, its contribution to CO_2 consumption does not seem to be relevant. The quantification of silicate weathering and related consumption of CO_2 was difficult, because the variability and thus the error range were substantial. The atmospheric carbon consumption by silicate weathering was estimated to lie in the range of 44–72 g C m^{-2} yr^{-1}. Summed up, the transformed soils have the potential to sequester or consume CO_2 in the range of about 110–360 g C m^{-2} yr^{-1}. Such high rates are only possible with irrigation of the transformed soils to keep plant growth at a high pace. With time the macroporosity and the size of the macropore networks decreased to

about half of its original value. Due to the rather sandy character of the applied crushed material, the soils were able to maintain their positive characteristics for agricultural use. Although soil transformations may exert positive effects on plant growth and carbon sequestration, caution is needed to prevent soil compaction or other damages to soils that trigger deterioration of both soil ecosystem services and soil quality. Furthermore, it should be kept in mind that soil transformation is only a symptomatic measure and the problem of excess CO_2 emission still remains.

Declaration of Competing Interest

The authors declare that they have no known competing financial interests or personal relationships that could have appeared to influence the work reported in this paper.

Acknowledgements

We would like to thank Gianluigi Ferro, Antonino Sciabbarrasi, Antonino Bilello, Matteo Mannino and Elio Clementi for giving access to the agricultural land, their help in the field and contribution to this work with valuable suggestions and discussions. We also thank Tatjana Kraut, Esmail Taghizadeh, Marion Rothaupt and Annette Röthlisberger for their support in the laboratory. We are grateful for the comments of two unknown reviewers on an earlier version of the manuscript.

Appendix A. Supplementary data

Supplementary data to this article can be found online at https://doi.org/10.1016/j.geoderma.2021.115355.

References

Aguilera, E., Lassaletta, L., Gattinger, A., Gimeno, B.S., 2013. Managing soil carbon for climate change mitigation and adaptation in Mediterranean cropping systems: A metaanalysis. Agric. Ecosyst. Environ. 168, 25–36. https://doi.org/10.1016/j.agee.2013.02.003.

Álvaro-Fuentes, J., López, M., Arrue, J., Moret, D., Paustian, K., 2009. Tillage and cropping effects on soil organic carbon in Mediterranean semiarid agroecosystems: Testing the Century model. Agricul. Ecosyst. Environ. 134, 211–217. https://doi.org/10.1016/j.agee.2009.07.001.

Álvaro-Fuentes, J., Plaza-Bonilla, D., Arrúe, J.L., Lampurlanés, J., Cantero-Martínez, C., 2014. Soil organic carbon storage in a no-tillage chronosequence under Mediterranean conditions. Plant Soil 376, 31–41. https://doi.org/10.1007/s11104-012-1167-x.

Amer, A.-M.-M., Logsdon, S.D., Davis, D., 2009. Prediction of hydraulic conductivity as related to pore size distribution in unsaturated soils. Soil Sci. 174, 508–515. https://doi.org/10.1097/SS.0b013e3181b76c29.

Andrews, M.G., Taylor, L.L., 2019. Combating climate change through enhanced weathering of agricultural soils. Elements 15, 53–258. https://doi.org/10.2138/gselements.15.4.253.

Angst, G., Messinger, J., Greiner, M., Häusler, W., Hertel, D., Kirfel, K., Kögel-Knabner, I., Leuschner, C., Rethemeyer, J., Mueller, C.W., 2018. Soil organic carbon stocks in topsoil and subsoil controlled by parent material, carbon input in the rhizosphere, and microbial-derived compounds. Soil Biol. Biochem. 122, 19–30. https://doi.org/10.1016/j.soilbio.2018.03.026.

Arnone, E., Pumo, D., Viola, F., Noto, L.V., La Loggia, G., 2013. Rainfall statistics changes in Sicily. Hydrol. Earth Syst. Sci. 17, 2449–2458. https://doi.org/10.5194/hess-17-2449-2013.

Bailey, E.H., Ragnarsdottir, K.V., 1994. Uranium and thorium solubilities in subduction zone fluids. Earth Planet. Sci. Lett. 124, 119–129. https://doi.org/10.1016/0012-821X(94)00071-9.

Birkeland, P.W., Burke, R.M., 1988. Soil catena chronosequences on eastern Sierra Nevada moraines, California, U.S.A. Arct Alp Res 20, 473–484.

Blättler, C.L., Higgins, J.A., 2017. Testing Urey's carbonate–silicate cycle using the calcium isotopic composition of sedimentary carbonates. Earth Planet. Sci. Lett. 479, 241–251. https://doi.org/10.1016/j.epsl.2017.09.033.

Breitenbach, S.F., Bernasconi, S.M., 2011. Carbon and oxygen isotope analysis of small carbonate samples (20 to 100 microg) with a GasBench II preparation device. Rapid Commun. Mass Spectrom. 25, 1910–1914.

Buggle, B., Glaser, B., Hambach, U., Gerasimenko, N., Markovic, S., 2011. An evaluation of geochemical weathering indices in loess-paleosol studies. Quat. Int. 240, 12–21.

Busacca, A.J., 1987. Pedogenesis of a chronosequence in the sacramento Valley, California, USA, I. Application of a Soil Development Index. Geoderma 41, 123–148.

Carnicelli, S., Mirabella, A., Cecchini, G., Senesi, G., 1997. Weathering of chlorite to a low-charge expandable mineral in a spodosol on the Apennine mountains, Italy. Clays Clay Miner. 45, 28–41.

Caruso, A., Pierre, C., Blanc-Valleron, M.-M., Rouchy, J.M., 2015. Carbonate deposition and diagenesis in evaporitic environments. The evaporative and sulphur-bearing limestones during the settlement of the Messinian Salinity Crisis in Sicily and Calabria. Palaeogeogr. Palaeoclimatol. Palaeoecol. 429, 136–162. https://doi.org/10.1016/j.palaeo.2015.03.035.

Chadwick, O.A., Brimhall, G.H., Hendricks, D.M., 1990. From a black to a gray box – a mass balance interpretation of pedogenesis. Geomorphology 3, 369–390. https://doi.org/10.1016/0169-555X(90)90012-F.

Chivenge, P., Murwira, H., Giller, K., Mapfumo, P., Six, J., 2007. Long-term impact of reduced tillage and residue management on soil carbon stabilization: Implications for conservation agriculture on contrasting soils. Soil Tillage Res. 94, 328–337. https://doi.org/10.1016/j.still.2006.08.006.

Clemente, E., 1990. Le sciare del Trapanese. Trasformazione, utilizzazione ed evoluzione dei substrati sotto l'influenza dell'irrigazione. MSc thesis, Istituto di Agronomia e Coltivazione Erbacee, Facoltà di Agraria. Università di Palermo.

Crescimanno, F.G., di Lorenzo, R., Occorso, G., Sottile I., Barbagallo, M.G., Raimondi, S., 1987. Influenza del rapporto grappoli su gemme sulla produzione dell'uva Italia coltivata in diversi tipi di terreno nel Canicattinese. In: Ministero Agricoltura e Foreste, Regione Siciliana, Ente di Sviluppo Agricolo, Istituto Sperimentale per la Frutticoltura di Roma, Istituto di Coltivazioni Arboree dell'Università di Palermo (Eds), Atti del Convegno nazionale sulle uve da tavola e uve apirene Canicattì (AG); 13–14 novembre 1986, Vicini Editore Roma, pp.123-149.

Dahms, D.E., 2002. Glacial stratigraphy of Stough Creek Basin, Wind River Range, Wyoming. Geomorphology 42, 59–83.

Dazzi, C., Galati, A., Crescimanno, M., Lo Papa, G., 2019. Pedotechnique applications in large-scale farming: Economic value, soil ecosystems services and soil security. Catena 181, 104072. https://doi.org/10.1016/j.catena.2019.104072.

Dignac, M.-F., Derrien, D., Barré, P., Barot, S., Cécillon, L., Chenu, C., Chevallier, T., Freschet, G.T., Garnier, P., Guenet, B., Hedde, M., Klumpp, K., Lashermes, G., Maron, P.-A., Nunan, N., Roumet, C., Basile-Doelsch, I., 2017. Increasing soil carbon storage: Mechanisms, effects of agricultural practices and proxies. A review. Agronomy Sustain. Develop. 37, 14. https://doi.org/10.1007/s13593-017-0421-2.

Döbelin, N., Kleeberg, R., 2015. Profex: a graphical user interface for the Rietveld refinement program BGMN. J. Appl. Crystallogr. 48, 1573–1580.

Egli, M., Fitze, P., 2000. Formulation of pedologic mass balance based on immobile elements: a revision. Soil Sci. 165, 437–443. https://doi.org/10.1097/00010694-200005000-00008.

Egli, M., Fitze, P., 2001. Quantitative aspects of carbonate leaching of soils with differing ages and climates. Catena 46, 35–62.

Egli, M., Fitze, P., Mirabella, A., 2001. Weathering and evolution of soils formed on granitic, glacial deposits: results from chronosequences of Swiss alpine environments. Catena 45, 19–47.

Egli, M., Favilli, F., Krebs, R., Pichler, B., Dahms, D., 2012. Soil organic carbon and nitrogen accumulation rates in cold and alpine environments over 1 Ma. Geoderma 183–184, 109–123.

Egli, M., Plötze, M., Tikhomirov, D., Kraut, T., Wiesenberg, G.L.B., Lauria, G., Raimondi, S., 2020. Soil development on sediments and evaporites of the Messinian crisis. Catena 187. https://doi.org/10.1016/j.catena.2019.104368.

Elmer, M., Gerwin, W., Schaaf, W., Zaplata, M.K., Hohberg, K., Nenov, R., Bens, O., Hüttl, R.F., 2013. Dynamics of initial ecosystem development at the artificial catchment Chicken Creek, Lusatia, Germany. Environ. Earth Sci. 69, 491–505. https://doi.org/10.1007/s12665-013-2330-2.

Ezzaïm, A., Turpault, M.-P., Ranger, J., 1999. Quantification of weathering processes in an acid brown soil developed from tuff (Beaujolais, France). Part 1 Formation of weathered rind. Geoderma 87, 137–154.

Frondini, F., Vaselli, O., Zuccolini, M.V., 2019. Consumption of atmospheric carbon dioxide through weathering of ultramafic rocks in the Voltri massif (Italy): Quantification of the process and global implications. Geosciences 9, 258. https://doi.org/10.3390/geosciences9060258.

FSKB (Fachverband der Schweizerischen Kies- und Betonindustrie), 2021. FSK-Rekultivierungsrichtlinie. Bern.

Gessesse, T.A., Khamzina, A., 2018. How reliable is the Walkley-Black method for analyzing carbon-poor, semi-arid soils in Ethiopia? J. Arid Environ. 153, 98–101. https://doi.org/10.1016/j.jaridenv.2018.01.008.

Gerwin, W., Schaaf, W., Biemelt, D., Winter, S., Fischer, A., Veste, M., Hüttl, R.F., 2011. Overview and first results of ecological monitoring at the artificial watershed Chicken Creek (Germany). Phys. Chem. Earth. 36, 61–73. https://doi.org/10.1016/j.pce.2010.11.003.

Gocke, M., Pustovoytov, K., Kuzyakov, Y., 2012. Pedogenic carbonate formation: Recrystallization versus migration – Process rates and periods assessed by 14C labeling. Global Biogeochem. Cycles 26, GB1018. https://doi.org/10.1029/2010GB003871.

Goodman, A.Y., Rodbell, D.T., Seltzer, G.O., Mark, B.G., 2001. Subdivision of glacial deposits in southeastern Peru based on pedogenetic development and radiometric ages. Quat. Res. 56, 31–50.

Harden, J.W., 1982. A quantitative index of soil development from field descriptions: examples from a chronosequence in central California. Geoderma 28, 1–28.

Hilley, G.E., Porder, S., 2008. A framework for predicting global silicate weathering and CO2 drawdown rates over geologic time-scales. PNAS 4, 16855-16859. 10.1073_pnas.0801462105.
Hirmas, D.R., Giménez, D., Nemes, A., Kerry, R., Brunsell, N.A., Wilson, C.J., 2018. Climate-induced changes in continental-scale soil macroporosity may intensify water cycle. Nature 561, 100–103. https://doi.org/10.1038/s41586-018-0463-x.
Hitz, C., Egli, M., Fitze, P., 2002. Determination of the sampling volume for representative analysis of alpine soils. Z. Pflanzenernährung und Bodenkunde 165, 326–331.
Hoogsteen, M.J., Lantinga, E.A., Bakker, E.J., Groot, J.C., Tittonell, P.A., 2015. Estimating soil organic carbon through loss on ignition: Effects of ignition conditions and structural water loss. European Journal of Soil Science 66 (2), pp. 320–328. 10.1111/ejss.12224.
IPCC (Intergovernmental Panel on Climate Change), 2020. Summary for Policymakers. In: Climate Change and Land: an IPCC special report on climate change, desertification, land degradation, sustainable land management, food security, and greenhouse gas fluxes in terrestrial ecosystems. P.R. Shukla, J. Skea, E. Calvo Buendia, V. Masson-Delmotte, H.- O. Pörtner, D. C. Roberts, P. Zhai, R. Slade, S. Connors, R. van Diemen, M. Ferrat, E. Haughey, S. Luz, S. Neogi, M. Pathak, J. Petzold, J. Portugal Pereira, P. Vyas, E. Huntley, K. Kissick, M. Belkacemi, J. Malley, (eds.), WMO, UNEP.
IUSS Working Group WRB, 2015. World reference base for soil resources, 2014. Update 2015. World Soil Resources Reports, Rome.
Jackson, R.B., Lajtha, K., Crow, S.E., Hugelius, G., Kramer, M.G., Piñeiro, G., 2017. The Ecology of Soil Carbon: Pools, vulnerabilities, and biotic and abiotic controls. Annu. Rev. Ecol. Evol. Syst. 48, 419–445. https://doi.org/10.1146/annurev-ecolsys-112414-054234.
Jarvis, N., 2007. A review of non-equilibrium water flow and solute transport in soil macropores: Principles, controlling factors and consequences for water quality. Eur. J. Soil Sci. 58, 523–546. https://doi.org/10.1111/j.1365-2389.2007.00915.x.
Jiang, P., Yu, G., Zhang, Q., Zou, Y., Tang, Q., Kang, Z., Sytharith, P., Xiao, H., 2020. Chemical weathering and CO2 consumption rates of rocks in the Bishuiyan subterranean basin of Guangxi, China. Scientific Reports 10, 11677. https://doi.org/10.1038/s41598-020-68572-4.
Kauer, K., Astover, A., Viiralt, R., Raave, H., Kätterer, T., 2019. Evolution of soil organic carbon in a carbonaceous glacial till as an effect of crop and fertility management over 50 years in a field experiment. Agric. Ecosyst. Environ. 283, 106562 https://doi.org/10.1016/j.agee.2019.06.001.
Kellogg, L.H., Lokavarapu, H., Turcotte, D.L., 2019. Carbonation and the Urey reaction. Am. Mineral. 104, 1365–1368. https://doi.org/10.2138/am-2019-6880.
Khedim, N., Cécillon, L., Poulenard, J., Barré, P., Baudin, F., Marta, S., Rabatel, A., Dentant, C., Cauvy-Fraunié, S., Anthelme, F., Gielly, L., Ambrosini, R., Fanzetti, A., Azzoni, R.S., Caccianiga, M.S., Compostella, C., Clague, J., Tielidze, L., Messager, E., Choler, P., Ficetola, G.F., 2020. Topsoil organic matter build-up in glacier forelands around the world. Glob. Change Biol. 00, 1–16. https://doi.org/10.1111/gcb.15496.
Kochiieru, M., Lamorski, K., Feiza, V., Feiziene, D., Volungevičius, J., 2018. The effect of soil macroporosity, temperature and water content on CO2 efflux in the soils of different genesis and land management. Zemdirbyste-Agriculture 105, 291–298. https://doi.org/10.13080/z-a.2018.105.037.
Köhler, P., Hartmann, J., Wolf-Gladrow, D., 2010. Geoengineering potential of artificially enhanced silicate weathering of olivine. Proc. Natl. Acad. Sci. 107, 20228–20233. https://doi.org/10.1073/pnas.1000545107.
Laban, P., Metternicht, G., Davies, J., 2018. Soil biodiversity and soil organic carbon: keeping drylands alive. Gland, Switzerland: IUCN. 10.2305/iucn.ch.2018.03.en.
Lanson, B., 1997. Decomposition of experimental X-ray diffraction patterns (profile fitting): a convenient way to study clay minerals. Clays Clay Miner. 45, 132–146.
Lichter, J., 1998. Rates of weathering and chemical depletion in soils across a chronosequence of Lake Michigan sand dunes. Geoderma 85, 255–282.
Liotta, M., Grassa, F., D'Alessandro, W., Favara, R., Gagliano Candela, E., Pisciotta, A., Scaletta, C., 2013. Isotopic composition of precipitation and groundwater in Sicily, Italy. Applied Geochemistry 34, 199-2056. 10.1016/j.apgeochem.2013.03.012.
Lombardo, V., Raimondi, S., 1991. Valore agronomico di substrati colturali ottenuti dalla trasformazione delle «sciare». Informatore Agrario 47, 53–59.
Luo, Z., Wang, E., Sun, O.J., 2010. Soil carbon change and its responses to agricultural practices in Australian agro-ecosystems: A review and synthesis. Geoderma 155, 211–223. https://doi.org/10.1016/j.geoderma.2009.12.012.
Lybrand, R.A., Rasmussen, C., 2015. Quantifying climate and landscape position controls on soil development in semiarid ecosystems. Soil Sci. Soc. Am. J. 79, 104–116.
McFadden, L.D., Weldon, R.J., 1987. Rates and Processes of Soil Development on Quaternary Terraces in Cajon Pass, Southern California. Geol. Soc. Am. Bull. 98, 280–293.
Mehlhorn, T., Prohaska, S., Homberg, U., Slowik, V., 2009. Modelling and Analysis of Particle and Pore Structures in Soils. Schriftenreihe Geotechnik 21, 53–60.
McKeague, J.A., Brydon, J.E., Miles, N.M., 1971. Differentiation of forms of extractable iron and aluminium in soils. Soil Sci. Soc. Am. Proc. 35, 33–38.
Minasny, B., Malone, B.P., McBratney, A.B., Angers, D.A., Arrouays, D., Chambers, A., Chaplot, V., Chen, Z.-S., Cheng, K., Das, B.S., Field, D.J., Gimona, A., Hedley, C.B., Hong, S.Y., Mandal, B., Marchant, B.P., Martin, M., McConkey, B.G., Mulder, V.L., O'Rourke, S., Richer-de-Forges, A.C., Odeh, I., Padarian, J., Paustian, K., Pan, G., Poggio, L., Savin, I., Stolbovoy, V., Stockmann, U., Sulaeman, Y., Tsui, C.-C., Vågen, T.-G., van Wesemael, B., Winowiecki, L., 2017. Soil carbon 4 per mille. Geoderma 292, 59–86. https://doi.org/10.1016/j.geoderma.2017.01.002.
Mizota, C., van Reeuwijk, L.P., 1989. Clay mineralogy and chemistry of soils formed in volcanic material in diverse climate regions. International Soil Reference and Information Centre, Soil Monograph, vol. 2. Wageningen.
Moore, D.M., Reynolds, R.C., 1997. X-ray diffraction and the identification and analysis of clay minerals, 2nd edition. Oxford University Press, New York.
Musso, A., Lamorski, K., Sławiński, C., Geitner, C., Hunt, A., Greinwald, K., Egli, M., 2019. Evolution of soil pores and their characteristics in a siliceous and calcareous proglacial area. Catena 182. https://doi.org/10.1016/j.catena.2019.104154.
Nemes, A., Rawls, W.J., Pachepsky, Y.A., 2005. Influence of organic matter on the estimation of saturated hydraulic conductivity. Soil Sci. Soc. Am. J. 69, 1330–1337. https://doi.org/10.2136/sssaj2004.0055.
Nesbitt, H.W., Young, G.M., 1982. Early Proterozoic climates and plate motions inferred from major element chemistry of lutites. Nature 299, 715–717.
Novara, A., Gristina, L., Sala, G., Galati, A., Crescimanno, M., Cerdà, A., Badalamenti, W., La Mantia, T., 2017. Agricultural land abandonment in Mediterranean environment provides ecosystem services via soil carbon sequestration. Sci. Total Environ. 576, 420–429. https://doi.org/10.1016/j.scitotenv.2016.10.123.
Oehlert, A.M., Swart, P.K., 2014. Interpreting carbonate and organic carbon isotope covariance in the sedimentary record. Nat. Commun. 5, 1–7. https://doi.org/10.1038/ncomms5672.
Porder, S., 2019. How Plants Enhance Weathering and How Weathering is Important to Plants. Elements 15, 241–246. https://doi.org/10.2138/gselements.15.4.241.
Raimondi, S., Sarno, M., 1999. L'attitudine dei principali suoli del territorio di Canicattì (AG) alla produzione dell'uva Italia. Atti del convegno Suoli e Colture in Ambiente Mediterraneo, Palermo 15–18 settembre 1999, Servizio Pedologico dell'Assessorato Agricoltura e Foreste della Regione Sicilia. Palermo, pp. 54–61.
Raimondi, S., Puccio, D., Egli, M., 2020. An extra-urban soil cadastre for Italy: a first guide for the introduction of soil information. Int. J. Environ. Quality – EQA 39, 1–10. https://doi.org/10.6092/issn.2281-4485/8680.
Ridler, T.W., Calvard, S., 1978. Picture thresholding using an iterative selection method. IEEE Trans. Syst. Man. Cybern. 8, 630–632. https://doi.org/10.1109/TSMC.1978.4310039.
Sauer, D., 2010. Approaches to quantify progressive soil development with time in Mediterranean climate—I, Use of field criteria. Journal of Plant Nutrition and Soil Science 173, 822–842.
Sauer, D., Wagner, S., Brückner, H., Scarciglia, F., Mastronuzzi, G., Stahr, K., 2010. Soil development on marine terraces near Metaponto (Gulf of Taranto, southern Italy). Quat. Int. 222, 48–63. https://doi.org/10.1016/j.quaint.2009.09.030.
Sauer, D., 2017. Soil development: numerical indices. In: The International Encyclopedia of Geography. Richardson, D., Castree, N., Goodchild, M.M., Kobayashi, A., Liu, W., Marston, R.A. (eds), John Wiley & Sons, Ltd., 10.1002/9781118786352.wbieg0909.
Scalenghe, R., Celi, L., Costa, G., Laudicina, A.V., Santoni, S., Vespertino, D., La Mantia, T., 2015. Carbon stocks in a 50-year-old Eucalyptus camaldulensis stand in Sicily, Italy. Southern Forests. J. Forest Sci. https://doi.org/10.2989/20702620.2015.1055541.
Schroeder, P.A., Melear, N.D., West, L.T., Hamilton, D.A., 2000. Meta-gabbro weathering in the Georgia Piedmont, USA: implications for global silicate weathering rates. Chem. Geol. 163, 235–245.
Schwertmann, U., Friedl, J., Stanjek, H., Schulze, D.G., 2000. The effect of clay minerals on the formation of goethite and hematite from ferrihydrite after 16 years' ageing at 25°C and pH 4–7. Clay Miner. 35, 613–623. https://doi.org/10.1180/000985500547034.
Singh, M., Sarkar, B., Sarkar, S., Churchman, J., Bolan, N., Mandal, S., Menon, M., Purakayastha, T.J., Beerling, D.J., 2018. Stabilization of soil organic carbon as influenced by clay mineralogy. Adv. Agron. 148, 33–84. https://doi.org/10.1016/bs.agron.2017.11.001.
Taylor, L.L., Beerling, D.J., Quegan, S., Banwart, S.A., 2017. Simulating carbon capture by enhanced weathering with croplands: An overview of key processes highlighting areas of future model development. Biol. Lett. 13, 20160868. https://doi.org/10.1098/rsbl.2016.0868.
Tolpeshta, I.I., Sokolova, T.A., Vorob'eva, A.A., Izosimov, Y.G., 2018. Transformation of Trioctahedral Mica in the Upper Mineral Horizon of Podzolic Soil during the Two-Year-Long Field Experiment. Eurasian Soil Sc. 51, 843–856 (2018). 10.1134/S1064229318050125.
Trumpy, E., Donato, A., Gianelli, G., Gola, G., Minissale, A., Montanari, D., Santilano, A., Manzella, A., 2015. Geothermics Data integration and favourability maps for exploring geothermal systems in Sicily, southern Italy. Geothermics 56. https://doi.org/10.1016/j.geothermics.2015.03.004.
Urey, H.C., 1952. On the Early Chemical History of the Earth and the Origin of Life. Proceedings of the National Academy of Sciences of the United States of America 38, 351–363. https://doi.org/10.1073/pnas.38.4.351.
Valkama, E., Kunypiyaeva, G., Zhapayev, R., Karabayev, M., Zhusupbekov, E., Perego, A., Schillaci, C., Sacco, D., Moretti, B., Grignani, C., Acutis, M., 2020. Can conservation agriculture increase soil carbon sequestration? A modelling approach. Geoderma 369, 114298. https://doi.org/10.1016/j.geoderma.2020.114298.
Vicente-Vicente, J.L., García-Ruiz, R., Francaviglia, R., Aguilera, E., Smith, P., 2016. Soil carbon sequestration rates under Mediterranean woody crops using recommended management practices: A meta-analysis. Agric. Ecosyst. Environ. 235, 204–214. https://doi.org/10.1016/j.agee.2016.10.024.
Vilmundardóttir, O.K., Gísladóttir, G., Lal, R., 2015. Soil carbon accretion along an age chronosequence formed by the retreat of the Skaftafellsjökull glacier, SE-Iceland. Geomorphology 228, 124–133. https://doi.org/10.1016/j.geomorph.2014.08.030.

Viola, F., Liuzzo, L., Noto, L.V., Lo Conti, F., La Loggia, G., 2014. Spatial distribution of temperature trends in Sicily. Int. J. Climatol. 34, 1–17. https://doi.org/10.1002/joc.3657.

White, A.F., Brantley, S.L., 2003. The effect of time on the weathering of silicate minerals: why do weathering rates differ in the laboratory and field? Chem. Geol. 202, 479–506.

White, A.F., Schulz, M.S., Lawrence, C.R., Vivit, D.V., Stonestrom, D.A., 2017. Long-term flow-through column experiments and their relevance to natural granitoid weathering rates. Geochim. Cosmochim. Acta 202, 190–214.

Wiesmeier, M., Urbanski, L., Hobley, E., Lang, B., Lützow, M.V., Marin-Spiotta, E., Wesemael, B.V., Rabot, E., Liess, M., Garcia-Franco, N., Wollschläger, U., Vogel, H.-J., Kögel-Knabner, I., 2019. Soil organic carbon storage as a key function of soils - A review of drivers and indicators at various scales. Geoderma 333, 149–162. https://doi.org/10.1016/j.geoderma.2018.07.026.

Wilson, M.J., 2004. Weathering of the primary rock-forming minerals: processes, products and rates. Clay Miner. 39, 233–266. https://doi.org/10.1180/0009855043930133.

Wright, V.P., Tucker, M.E., 1991. Calcretes: an introduction. Int. Assoc. Sedimentol. Reprint Series 2, 1–22.

Yang, Y., Wu, J., Zhao, S., Han, Q., Pan, X., He, F., Chen, C., 2018. Assessment of the responses of soil pore properties to combined soil structure amendments using X-ray computed tomography. Sci. Rep. 8, 695. https://doi.org/10.1038/s41598-017-18997-1.

Zhang, G., Germaine, J.T., Martin, T., Whittle, A.J., 2003. A simple sample-mounting method for random powder X-ray diffraction. Clay Clay Miner. 51, 218–225. https://doi.org/10.1346/CCMN.2003.0510212.